Sensor and Simulation Notes

Note 475

June 2003

Characterization of a Time Domain Antenna Range

Lanney M. Atchley, Everett G. Farr, Leland H. Bowen, W. Scott Bigelow,
Harald J. Wagnon, and Donald E. Ellibee
Farr Research, Inc.

Tyrone C. Tran
Air Force Research Laboratory / DE

Abstract

We characterize here the performance of a time domain antenna range by measuring a number of antennas, comparing the results to frequency domain measurements. Our time domain antenna range consists of a fast pulser and a sampling oscilloscope. We have demonstrated good performance of this range for all types of antennas (resonant and non-resonant) that operate between 900 MHz and 20 GHz. Furthermore, if the antenna is non-resonant, then good performance is observed as low as 200 MHz. Finally, it seems likely that by using a longer time window we can extend below 900 MHz the bandwidth of the antenna range for resonant antennas.

Table of Contents

I. Introduction

In this note we begin the process of characterizing our time domain antenna range, which is based on a fast pulser and a digital sampling oscilloscope. This system was originally described in [1]. Our approach here is to measure a number of antennas in the time domain, and then compare the results to frequency domain measurements obtained elsewhere.

Time domain antenna ranges seem to have a number of advantages over their frequency domain counterparts. First, the equipment is less expensive, i.e., a sampling oscilloscope and fast pulser are less expensive than a vector network analyzer (VNA). Second, our system is simple to set up for temporary use, so dedicated real estate is not required. Finally, our system can operate over a broad temperature range. This contrasts somewhat with a typical VNA, which must remain within a very narrow temperature range to avoid losing calibration.

Characterizing an antenna range is a challenging undertaking, because the performance of the range may be expected to depend upon a large number of variables. First, we expect performance to be dependent upon the characteristics of the ground at the outdoor range. Second, we expect it to be dependent upon the frequency range of the antennas under test. Finally, it is dependent upon the class of antenna that is measured. Highly resonant antennas that ring out to late times require measurements with long time windows. At such late times, it becomes impossible to time-gate out the effects of ground bounce. Furthermore, long time windows include more system noise than short time windows. On the other hand, Ultra-Wideband (UWB) antennas with little or no ringing allow one to time-gate out the effects of ground bounce quite nicely. For that reason, our range is especially well suited to measuring UWB antennas. However, as we will see, it also does well with a wide variety of more conventional antennas.

Because of the many variables described above, it is unclear how to fully characterize an antenna measurement system. Therefore, we have assembled a *potpourri* of antennas to characterize and we compare these results to frequency domain measurements. We hope that the measurements provided here will give a good feel for the accuracy of our system.

We begin this paper by describing the hardware included in the time domain antenna range. We then describe measurements of two Farr Research Impulse Radiating Antennas, with frequency range of 250 MHz to 20 GHz. This is followed by measurements of an EMCO 3115 ridged horn waveguide antenna, operating between 1 and 18 GHz. Then, we measure an EMCO 3147 Log Periodic Dipole Array, operating between 200 MHz and 5 GHz. Next, we measure a number of printed-circuit Log-Periodic Dipole Arrays, operating between 1 and 12 GHz. We then characterize a number of resonant Yagi and folded dipole antennas, in order to determine the range performance at lower frequencies. Finally, we characterize a Narda Model 640 X-band horn.

In the appendices of this paper, we summarize all the equations used in the antenna range to process the data.

Let us begin now by describing the experimental setup.

II. Hardware

The measurement system is the same as that described in [1], and as shown in Figure 2.1. A Farr Research model TEM-1-100 sensor was driven by a Picosecond Pulse Laboratory (PSPL) Model 4015C pulse generator (4 volts peak, 20 ps risetime). In one case, a PSPL Model 2000D generator (48 volts peak, 350 ps risetime) was substituted for the 4015C. The signal received by the Antenna Under Test (AUT) is detected by a Tektronix TDS8000 digital sampling oscilloscope (DSO) with an 80E04 sampling head.

It is apparent from Figure 2.1 that the separation between the transmitter and receiver can be known only approximately, because of the size of the antenna under test. This is especially true when the AUT is a Log-Periodic Dipole Array, which has a different phase center for each frequency. If the separation between the TEM-1-100 and the antenna under test becomes small, the size of both the AUT and the TEM-1-100 sensor may become an appreciable fraction of the separation.

Note that Figure 2.1 does not show azimuth/elevation positioners or computer control. We are in the process of adding these features and integrating the system into a single unit. The data presented here was taken in various stages of completion. Every effort has been made to minimize the effects of the tripod or antenna mast used to make the measurements.

The equations used in the analysis of the raw data are provided in Appendices A through D.
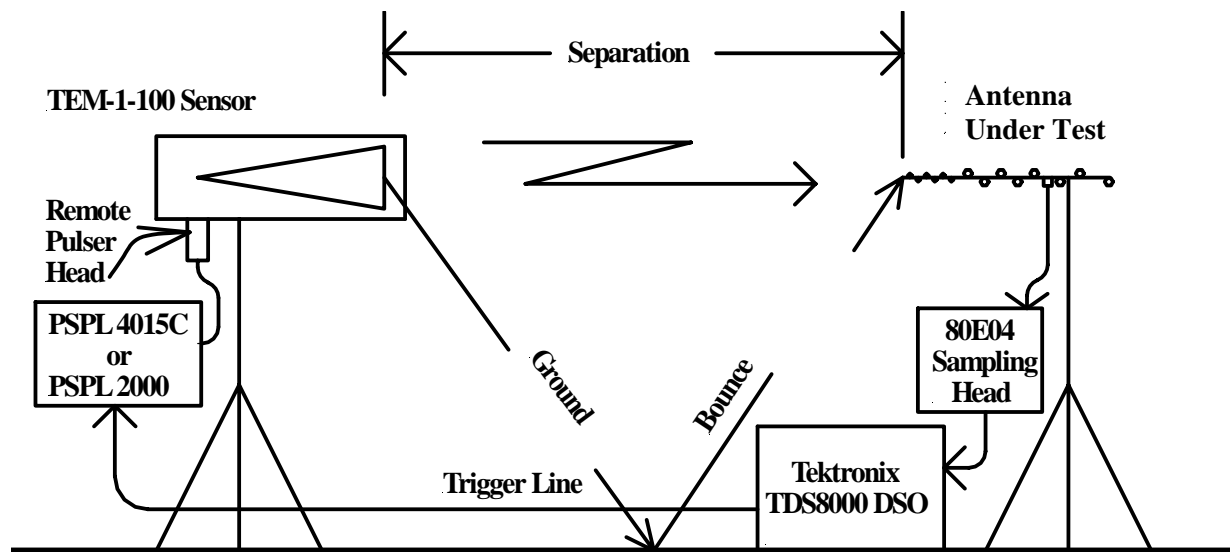

Figure 2.1. Measurement setup.

III. Measurements of Two Farr Research IRAs

We compare here our measurements of two Farr Research, Inc. (FRI) IRAs to measurements made by Raven Engineering and Mission Research Corporation. Photos of the two antennas are provided in Figure 3.1.
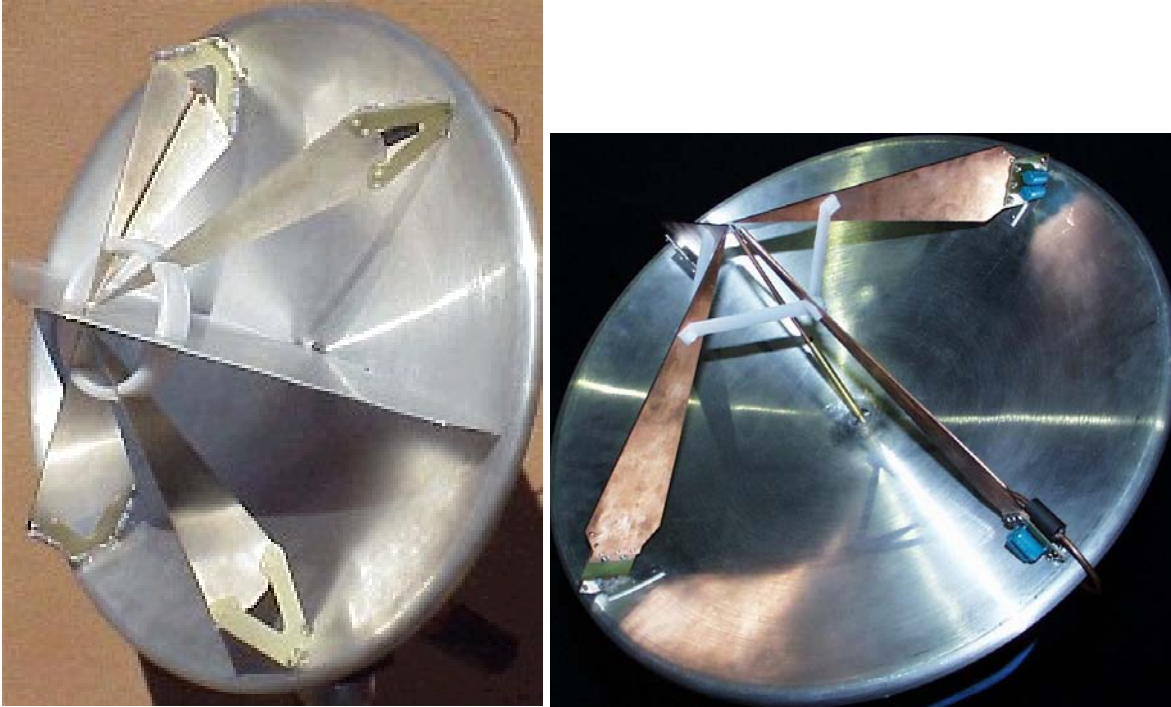

Figure 3.1. IRA-3 (left) and IRA prototype (right).

We sent two IRA-3s to Raven Engineering for MIL-STD-462 calibration of boresight gain. To simulate our range conditions, Raven tested the antennas at a height of 3 meters above a lossy-earth ground, with transmitting and receiving antennas separated by 10 meters. Raven measured IRA-3, serial number 4, using the second IRA-3, serial number 6, as the transmitting antenna. To process the data, they had to assume that the two antennas were identical, which was a reasonable assumption in this case.

In Figure 3.2 we compare the Raven gain measurement of IRA-3 to our time domain measurements of another IRA-3. We observe quite good agreement over the entire band, from 200 MHz to 20 GHz. The difference in gain is less than 2 dB for the entire frequency range.

Next, we compare our time domain measurements to those made on a frequency domain range located at Mission Research Corporation, in Dayton Ohio. The measurements are of an early prototype IRA (Figure 3.1, right), with feed arms positioned at ±45˚ to vertical, and with an 18-inch diameter aluminum reflector. The boresight gain is shown in Figure 3.3 for both time domain (Farr Research) and frequency domain (Mission Research) measurements. Once again, the data overlay nicely as high as they go, which is 10 GHz. For almost all of the frequency range, the two data sets are within 2 dB of each other.

To summarize, we compared our time domain measurements of an IRA to frequency domain measurements made by Raven and MRC, and we obtained excellent agreement from 200 MHz to 20 GHz.

Comparison of IRA and FRI Gain on the IRA-3

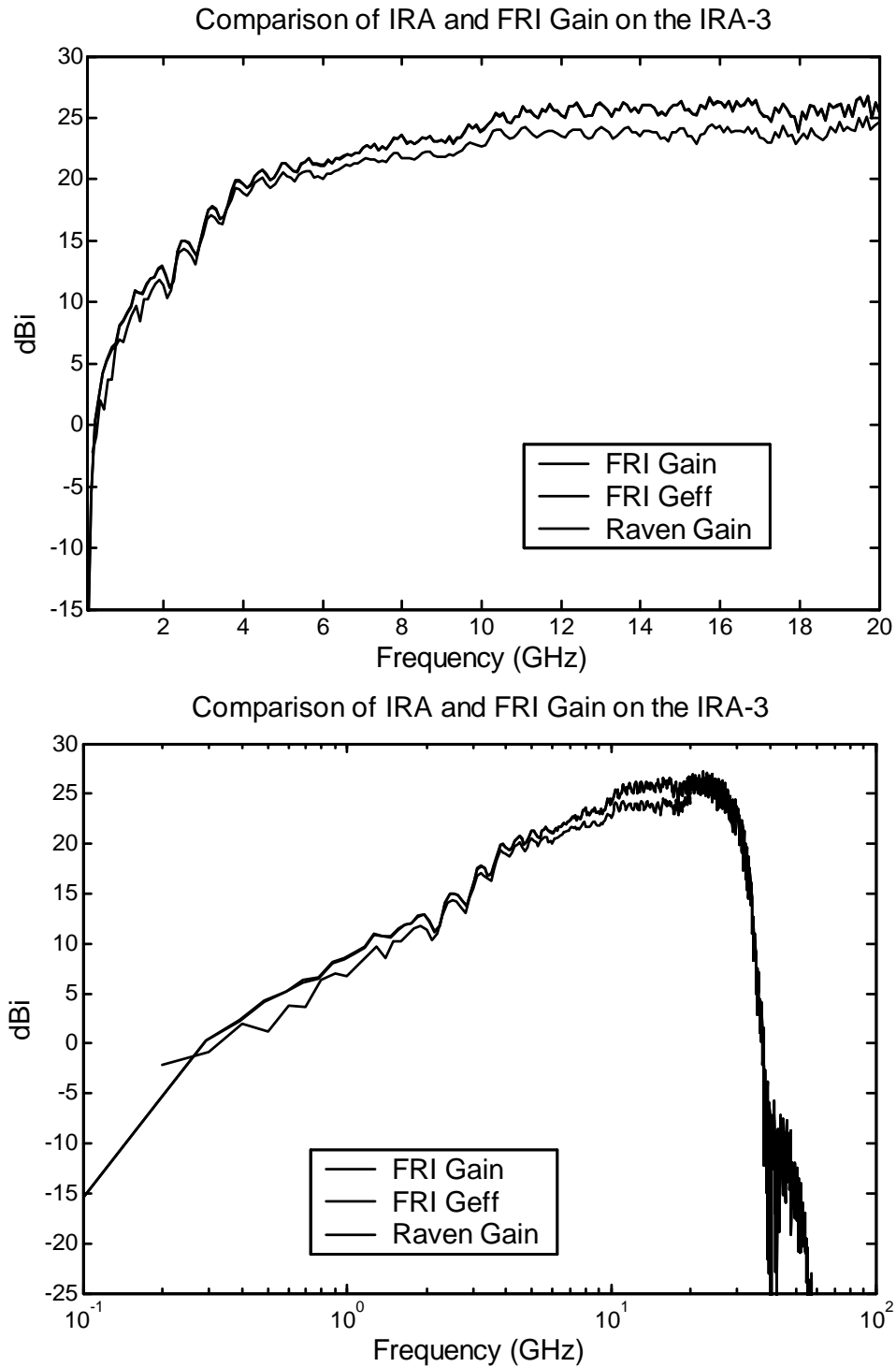Comparison of IRA and FRI Gain on the IRA-3

Figure 3.2. Comparison of Raven and Farr Research boresight gain measurements of IRA-3 antennas. Note that the FRI gain and effective gain plots (top) are indistinguishable from each other because they overlay almost exactly.
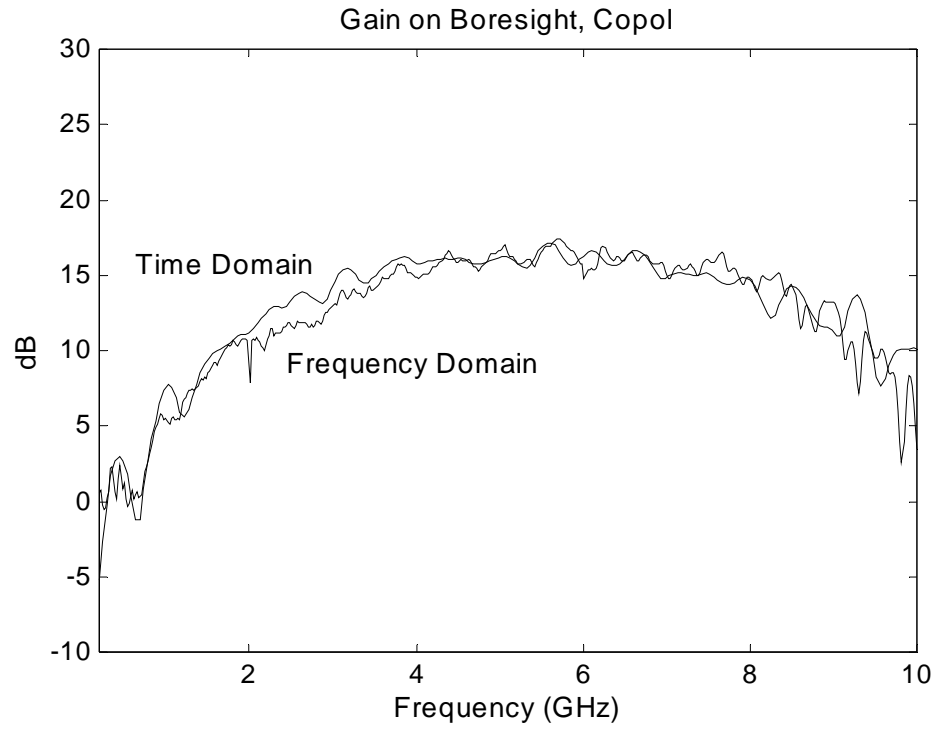
6

Figure 3.3. Comparison of the gain of the Prototype IRA on boresight, from time domain (FRI) and frequency domain (MRC) data.

IV Measurements of the EMCO 3115 Double-Ridged Waveguide Horn

We provide here measurements of the EMCO model 3115 double-ridged waveguide horn using our time domain antenna range, Raven Engineering's frequency domain range, and calibration data provided by the manufacturer (EMCO). Photos of the EMCO 3115 are provided in Figure 4.1.
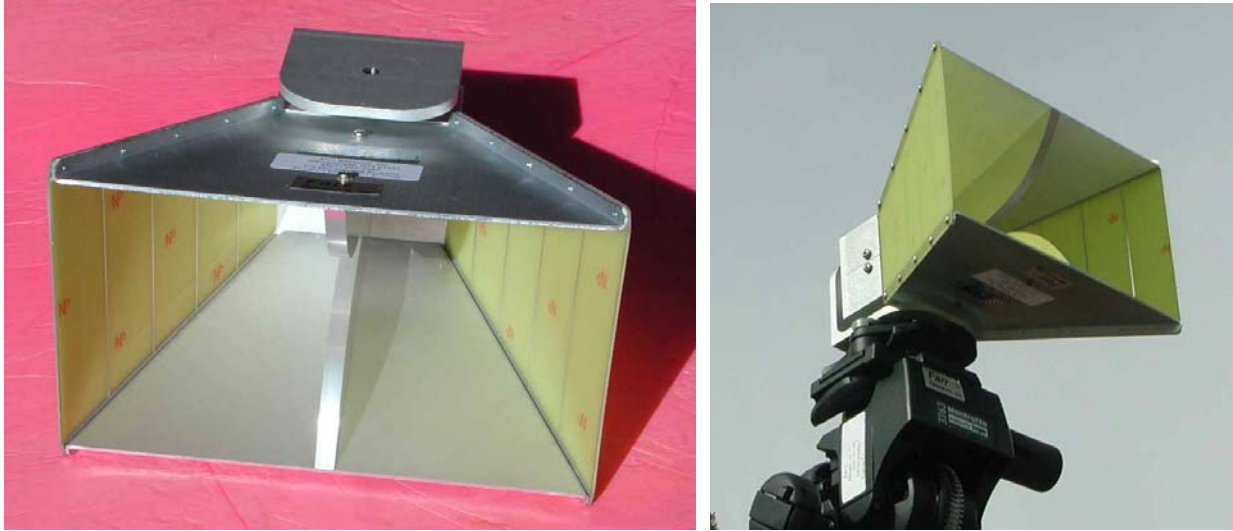

Figure 4.1. EMCO 3115 double-ridged waveguide horn.

A Far Field Determination

We measured the gain of the 3115 at 1 and 10 meters from the transmitting TEM sensor. EMCO provided gain calibration data with the antenna, measured according to the SAE ARP958 standard. This requires that gain be measured with two identical antennas, separated by one meter. It is important to note that this is a near-field measurement, as determined by the usual far-field criteria of

$$R > 2D^2 / \lambda$$
$$R \gg \lambda \tag{1}$$
$$R \gg D$$

Here, R is the distance from the horn, D is the largest dimension (0.28 meter) of the horn normal to the direction of propagation, and λ is the wavelength. The 1-meter distance is within the near field for nearly the entire frequency range of the antenna (f = 1 to 18 GHz, λ = 0.3 to 0.017 m), as determined by the first and third criteria. All three far-field criteria are satisfied only for $R >$ 9.4 m. Since the antenna response is different in the near field than in the far field, we measured the gain at one meter to match the EMCO calibration data and at 10 meters to record the far field gain.

B Farr Research and EMCO Gain Measurements

We now compare our gain measurements of the 3115 horn to EMCO's calibration data. In Figure 4.2, we provide our effective gain measurements at 1 and 10 meters, and compare to EMCO's calibration gain data at 1 meter. We observe good agreement between our data and EMCO's calibration data at 1 meter. Note that our data is plotted in terms of effective gain, whereas EMCO has provided gain as defined by the IEEE. The relationship between the two is

$$G_{eff}(\omega) \;=\; G(\omega)\left[1-|S_{11}|^2\right] \tag{2}$$

where $G(\omega)$ is gain as defined by IEEE, $G_{eff}(\omega)$ is the effective gain, and $S_{11}(\omega)$ is the standard scattering parameter looking into the antenna. For well-matched antennas such as the 3115, the difference between the two gains is very small.
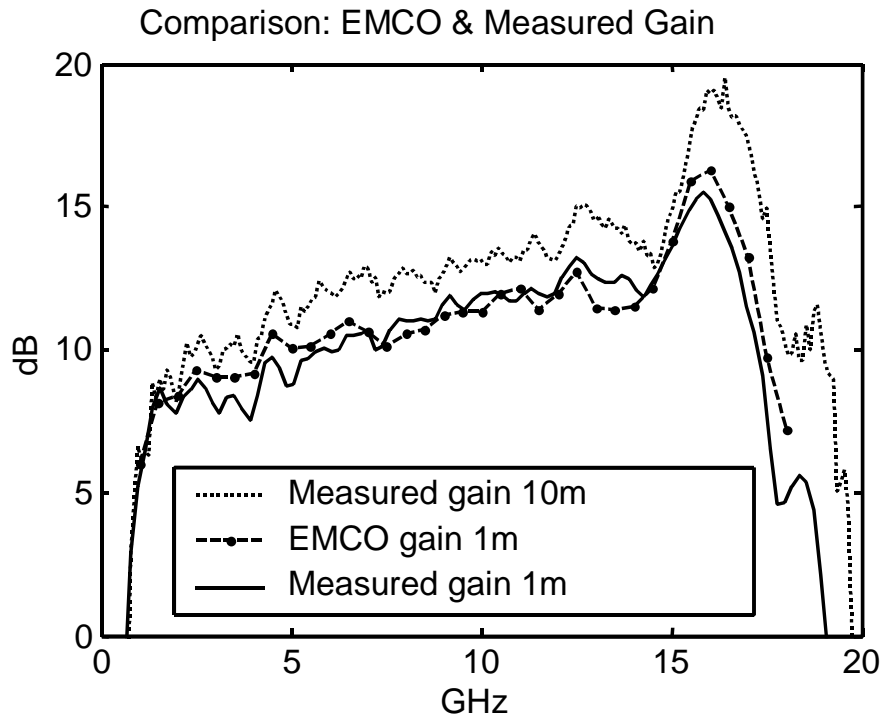

Figure 4.2. Comparison between EMCO calibration gain and FRI effective gain.

Next, we correct our data above so that we are overlaying IEEE gain in both graphs. Using the TDR data of the antenna, we can calculate the S_{11} of the antenna to correct for the difference between IEEE gain and effective gain. The correction factor is shown in Figure 4.3, and we see that it is less than 0.5 dB for the frequency range considered. We use this to convert our effective gain to IEEE gain, and we overlay the results with the calibration data in Figure 4.4. We observe good agreement between the two data sets.
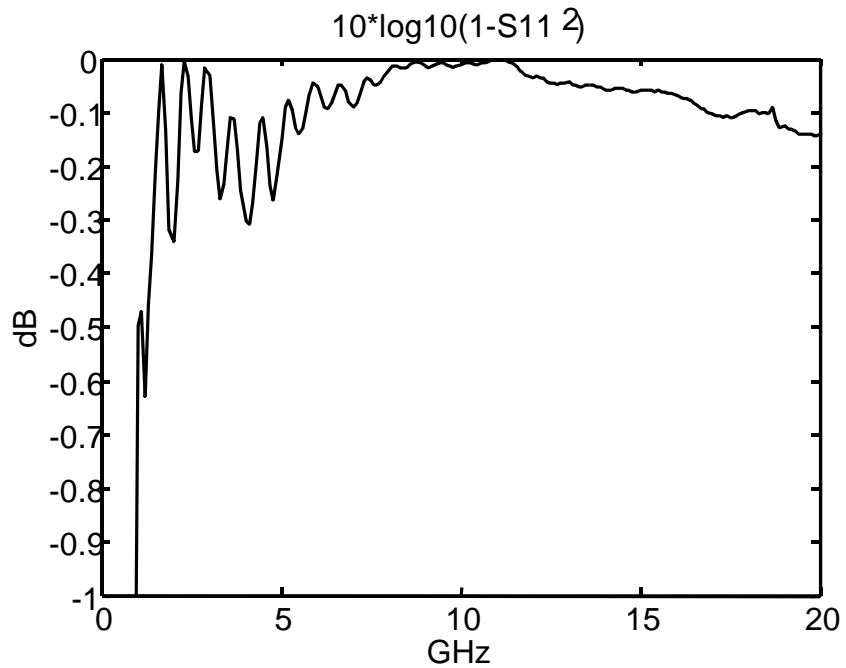
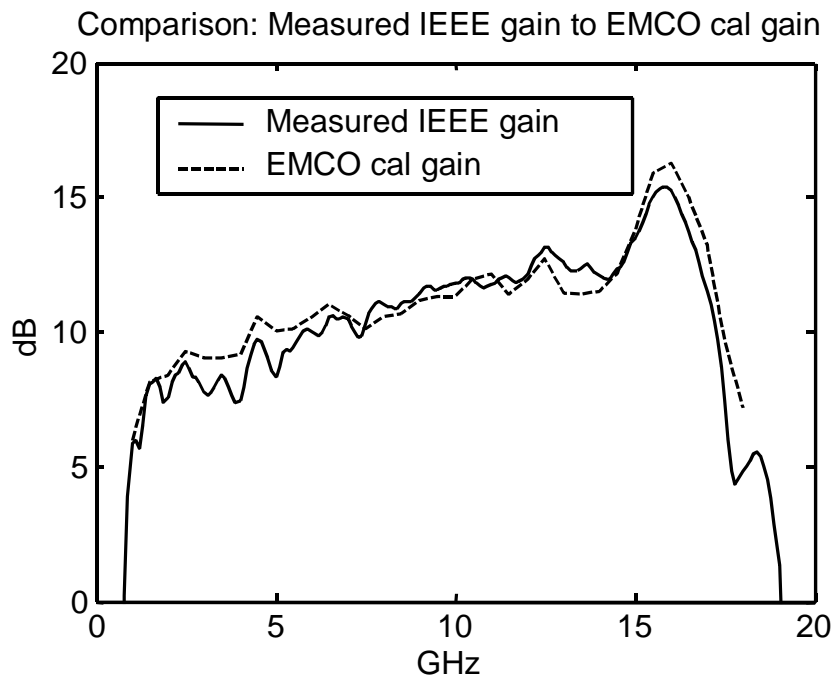Figure 4.3. Detail of the correction factor, $(1 - |S_{11}|^2)$.

Figure 4.4. Comparison of the EMCO 3115 1-meter gain measured two ways: 1) EMCO measured IEEE gain, and 2) FRI measured IEEE gain that is corrected using measured TDR data.

Finally, we calculate the normalized impulse response of the 3115 from our time domain data, as shown in Figure 4.5. Since we don't have any data for comparison, we do this only for our own information about the ridged horn. It has quite a narrow impulse response, with a FWHM of around 53 ps.
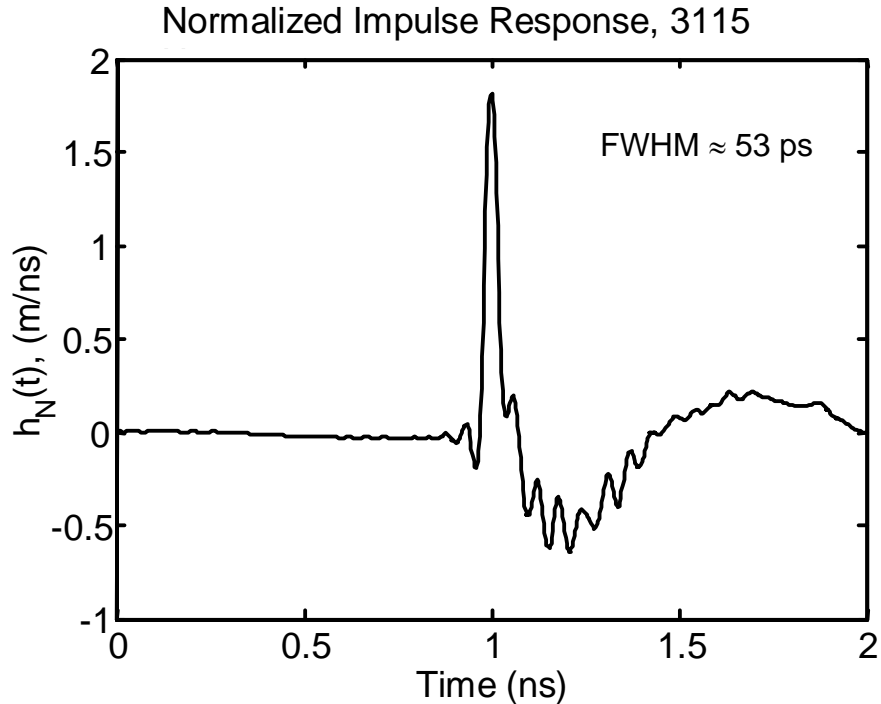

Figure 4.5. EMCO 3115, normalized impulse response measured on the FRI antenna range.

C Farr Research and Raven Engineering Gain Measurements

We sent the EMCO 3115 horn to Raven Engineering for calibration according to MIL-STD-462. To simulate our range conditions, Raven tested the horn at a height of 3 meters over dry earth, with transmitter-receiver separations of 3 and 10 meters. We provide Raven's measurements on the 3115, and we compare them both to our measured results and to EMCO's calibration data.

Raven measured the EMCO 3115 gain at separation distances of 3 and 10 meters, obtaining the results shown in Figure 4.6. The ten-meter measurement has slightly higher gain, which we attribute to differences between the far-field and near-field characteristics. We observed a similar effect in our own measurements at the FRI test range. Note that our purpose in having Raven make these measurements was to get a reliable ten-meter calibration for the double-ridged horn. EMCO provided only one-meter calibration data. Raven's three-meter data is for future comparisons.
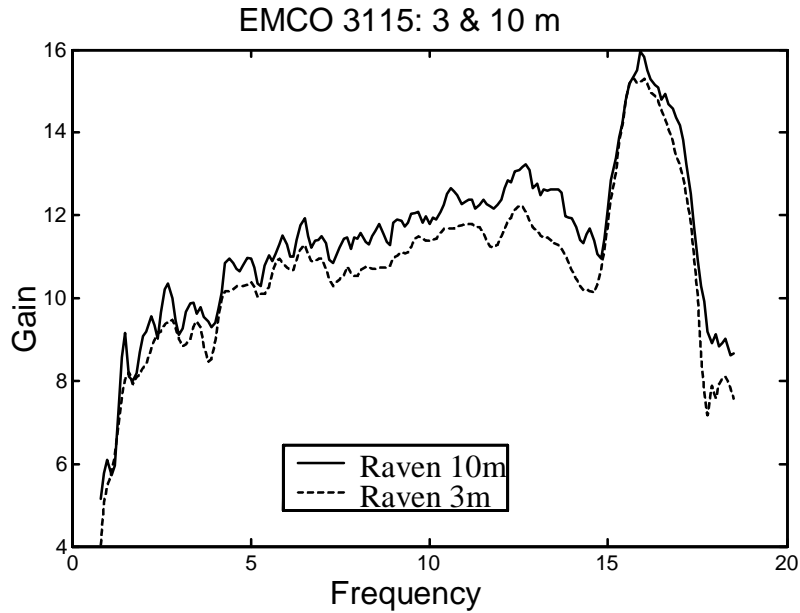
Figure 4.6. Raven-measured gain of the EMCO 3115 at 3 and 10 m.

We now overlay the gain of the EMCO 3115 at 10 meters as measured by FRI and Raven. The results are shown in Figure 4.7, and EMCO's one-meter gain is included for reference. The Raven and FRI 10-meter data disagree by only about two or three decibels at the high-frequency end, and the agreement is better at lower frequencies. Surprisingly, the Raven 10-meter data are actually a better match to the EMCO 1-meter data.
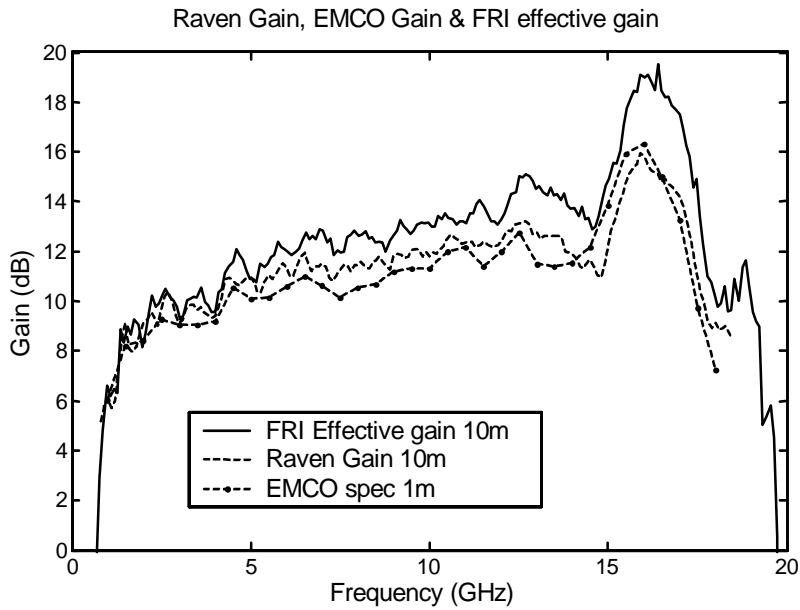
Figure 4.7. EMCO 3115 gain comparisons.

D Conclusions on the EMCO 3115 Measurements

We observe excellent agreement between our measurements and the EMCO calibration data. While this is in the near field for most of the frequency range, these data are still useful in confirming the measurement technique. At a distance of ten meters, our data are compared to the data from Raven. We see a bit higher discrepancy at 10 meters, but we believe the EMCO data is more reliable than the Raven data. This suggests to us that our measurements are accurate to about 2 dB over the entire antenna range.

V. Measurements of the EMCO 3147 Log Periodic Dipole Array

The EMCO 3147 is a challenging antenna to measure in the time domain, because of its highly resonant low-frequency response (between 200 MHz and 5 GHz). We observe a time domain signal that rings for around 500 ns, so there is some art to deciding where to truncate the signal. Here we compare the manufacturer's (EMCO's) own measurements and Raven Engineering's measurements to our time domain antenna range measurements. Photos of the EMCO 3147 are provided in Figure 5.1.
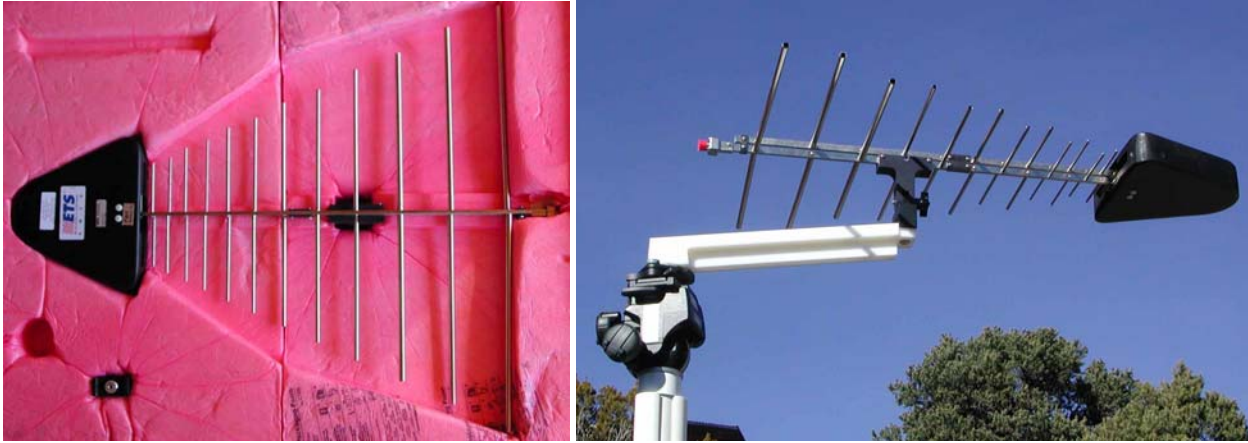

Figure 5.1. EMCO 3147 Log-periodic dipole array.

A Farr Research and EMCO Gain Measurements at 10-meter Separation

First we measured the gain of the EMCO 3147 while varying the time window. The complete raw waveform is shown in Figure 5.2, which demonstrates that a 500-nanosecond window is needed to capture the complete waveform. The results for gain are shown in Figure 5.3 as a function of window size. The first four plots: (a), (b), (c), and (d), show the gains for 50-ns, 100-ns, 200-ns, and 500-ns time windows respectively. The fifth plot, (e), is an overlay of the first four. The plots include an overlay of the gain at 10 meters, as provided by EMCO.

Our measured effective gain is reasonably independent of the acquisition window size, although agreement with the EMCO data at higher frequencies improves as the duration increases. Since all the time windows contain 4000 samples, the time between samples varies from 12.5 ps to 125 ps. Note that the oscillations below 2 GHz are spaced about 160 MHz apart. This is very close to the 170 MHz suggested by the time difference between the direct signal path and the ground-bounce path. This suggests that the periodic oscillations below 2 GHz are due to ground-bounce.
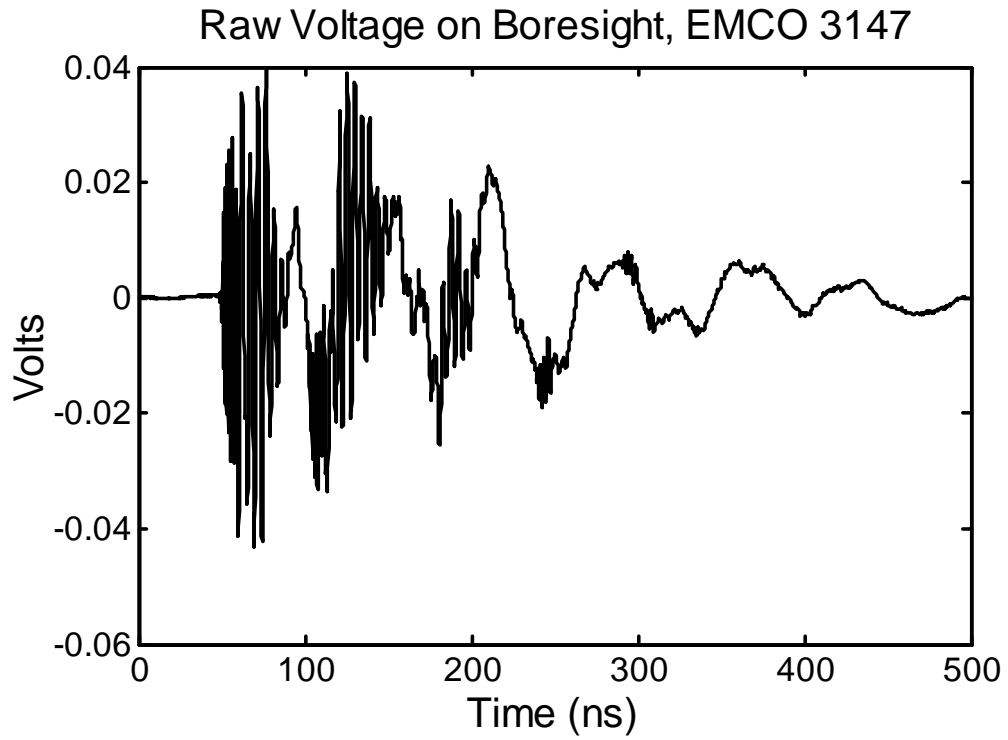
Figure 5.2 Raw voltage of the EMCO 3147 LPDA measurement, illustrating the very large time window required to capture the entire waveform.
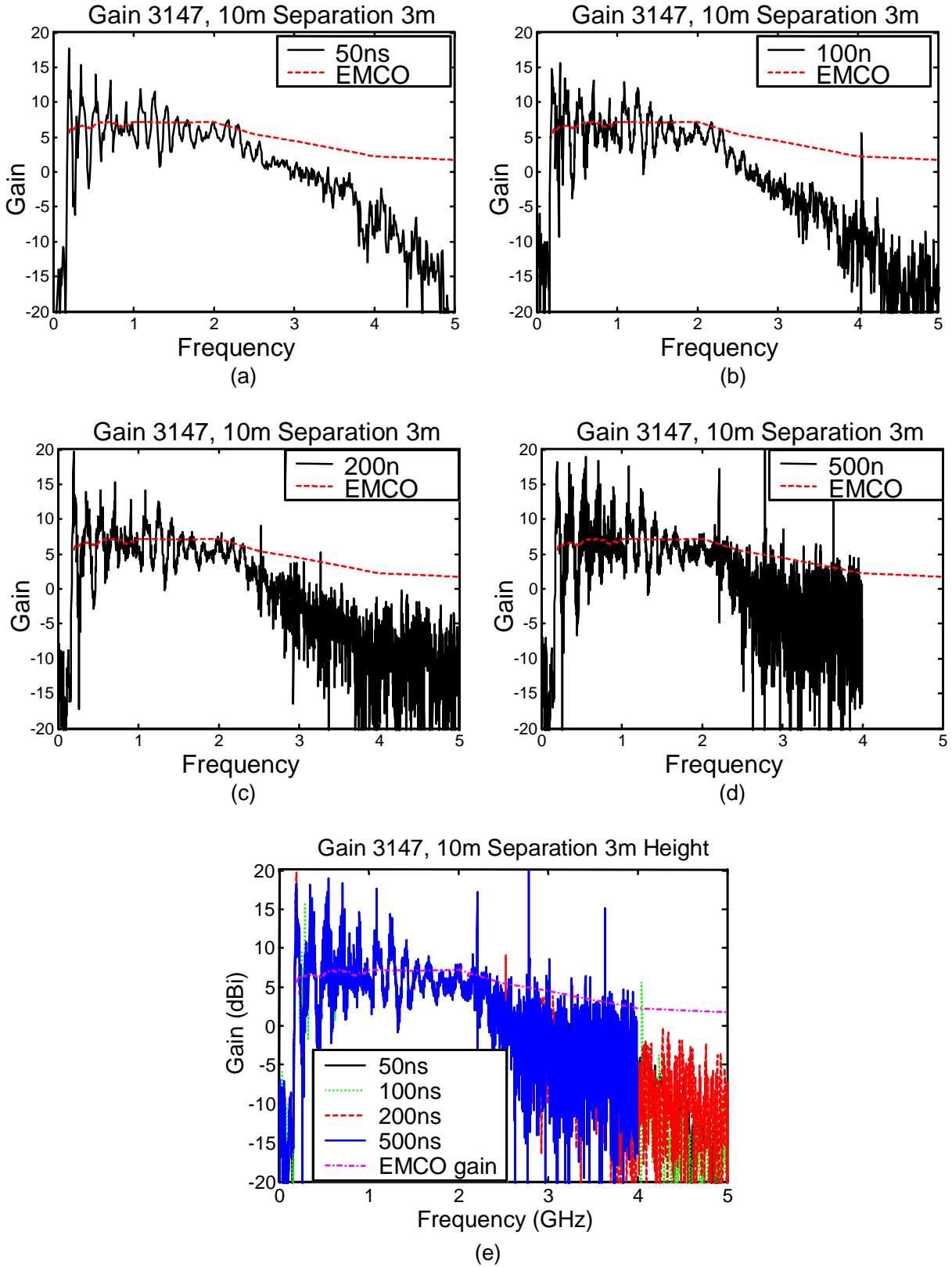
Figure 5.3. EMCO 3147 gain as measured with different acquisition time windows. The time windows are 50 ns (a), 100 ns (b), 200 ns (c), 500 ns (d), and an overlay of all four (e).

B Farr Research and EMCO Gain Measurements at 3-meter Separation

To further resolve the discrepancies in our gain measurements, we tested the EMCO 3147 log-periodic dipole array at a nominal three-meter separation from the transmitter, with two different pulse generators. The three-meter separation was actually 2.7 meters as measured from the tip of the log-periodic to the edge of the upper plate of the TEM-1-100 sensor. The effective distance between the log-periodic and the TEM-1-100 depends on which element of the log-periodic is active, as the nearly 1-meter length of the log-periodic dipole array is an appreciable fraction of the 3-meter spacing.

The first comparison, presented in Figure 5.4, is of the antenna gain measured at a 3-meter separation and 2.8-meter elevation. Here we used two different pulse generators and a 50-nanosecond time window. We used the PSPL 4015C (dashed trace) and the PSPL 2000D (solid trace). With the PSPL-2000D, we hoped to improve the characterization of the low frequency response. The EMCO calibration gain data is indicated by the dotted trace.

These data show that pulse generator selection is important. The PSPL 2000D produces less apparent high-frequency gain than the PSPL 4015C, whereas the PSPL 4015C seems adequate for the low frequency range. All the data agree fairly well below 1 to 2 GHz. This suggests that the faster 4015C was more suitable for this measurement.

The path length difference between a direct ray and a ground-bounce ray corresponds to about an 11-ns delay or a 90-MHz frequency shift for this setup. There is no clear 90 MHz oscillation in the data. We attribute this lack of an identifiable ground-bounce frequency to the geometry of the setup. The ground-bounce path is well outside the main beam of the TEM-1-100 sensor, so there is little signal radiated in that direction. We made these measurements inside a building where nearby reflection sources may account for the structure in the frequency response.
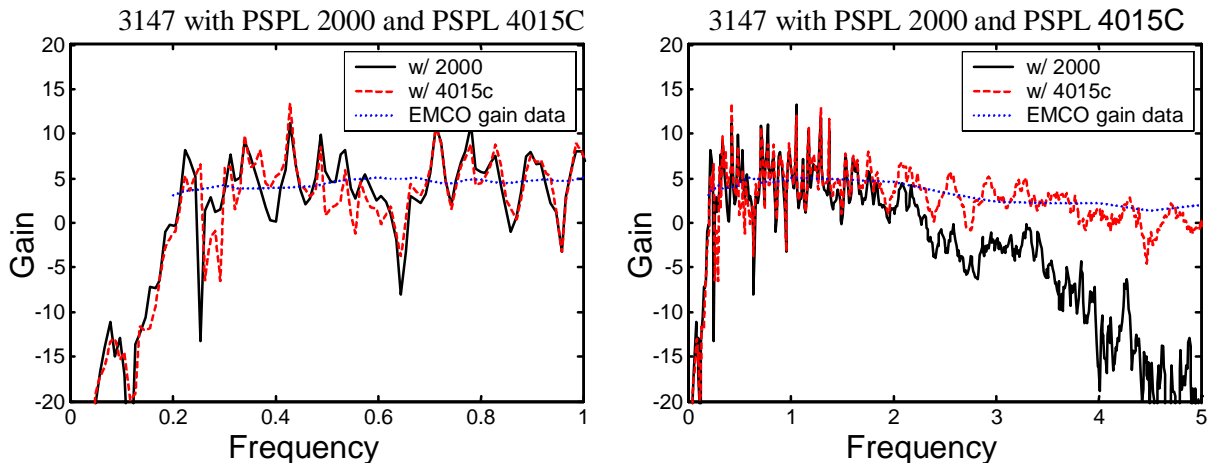

Figure 5.4. Comparison of the data taken with the PSPL 4015c to the PSPL 2000D.

Next we compare our data taken at a 10-meter separation and 3-meter height to data taken at a 3-meter separation and a 2.8-meter height. The results are shown in Figure 5.5. The two traces exhibit significant variation in structure, indicating that the gain measurement of the EMCO 3147 is dependent on separation and location. Note that the corresponding EMCO data at 3 meters and 10 meters overlay with each other nicely, while our data do not.
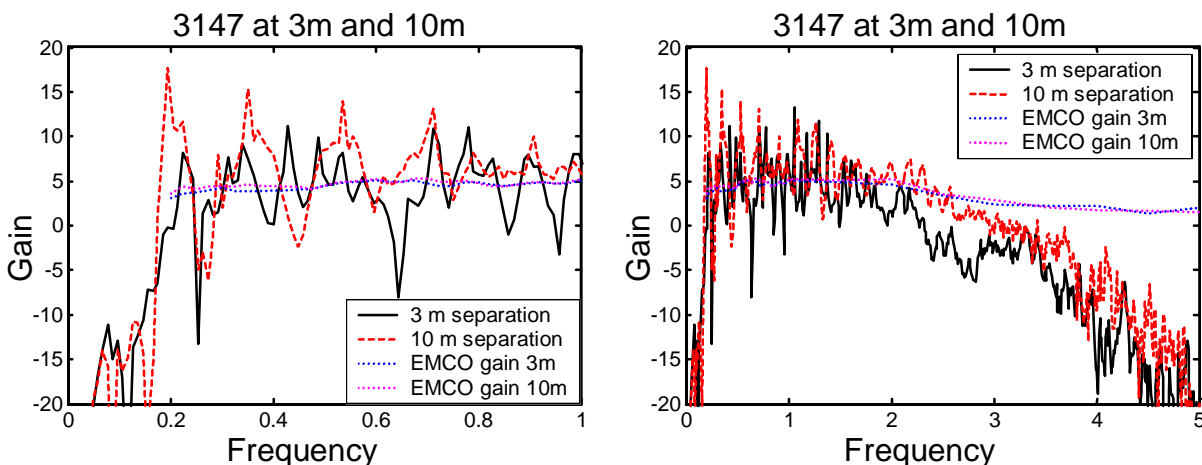

Figure 5.5. Comparison of EMCO log-periodic gain as measured at different separations and locations. Reflections from nearby objects may contribute to the additional structure in the 3-m indoor data.

C. Farr Research and Raven Gain Measurements

Raven measured the gain of the EMCO 3147 log-periodic dipole array at 3 and 10 m distances from the transmitter. The results are shown in Figure 5.6. The ten-meter measurement shows a pronounced oscillation in the frequency spectrum, which we attribute to ground bounce. The data taken at a distance of 3 meters does not have the oscillation, which suggests that it should be possible to obtain reasonable data at an outdoor range, if the correct distance is used.

Since all measurements are at a height of three meters, the difference in path length between a direct ray at 10-meter separation and the ground-bounced ray is 1.66 meters. That path length difference corresponds to about 180 MHz. Every multiple of that path length difference gives rise to a cycle of constructive and destructive interference between direct and reflected rays, resulting in a periodic oscillation in gain at about 180 MHz in the frequency domain.

The observed frequency of oscillation in the 10-meter Raven measurements of the EMCO 3147 is about 170 MHz. We attribute the difference between the observation and the calculation of 180 MHz to the ambiguity in identifying the reception location of the large log-periodic antenna. We see no ground-bounce oscillations at the 3-meter separation, presumably because the ground-bounce ray path is too far out of the main antenna lobes to contribute significantly.

Next, we compare the Raven-measured gains to the EMCO gains. In Figure 5.7 we provide the two gains at a ten-meter separation between the transmitting and receiving antennas. In Figure 5.8, we provide the same data at a 3-meter separation. The Raven measurements agree

well with the EMCO calibrations. The 10-meter measurement, which has a clear ground-bounce, agrees to within 6 dB. The 3-meter measurement, with fewer reflections, agrees to within about 3 dB. These measurements point out the challenge of making accurate measurements in the presence of reflections at low frequencies on resonant antennas.
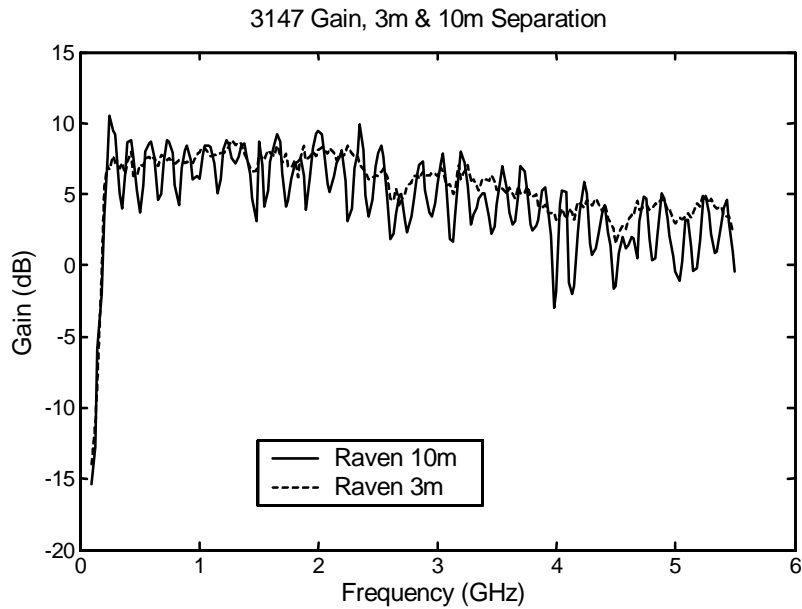
Figure 5.6. Raven-measured gain of the EMCO 3147 at distances of 3 and 10 m.
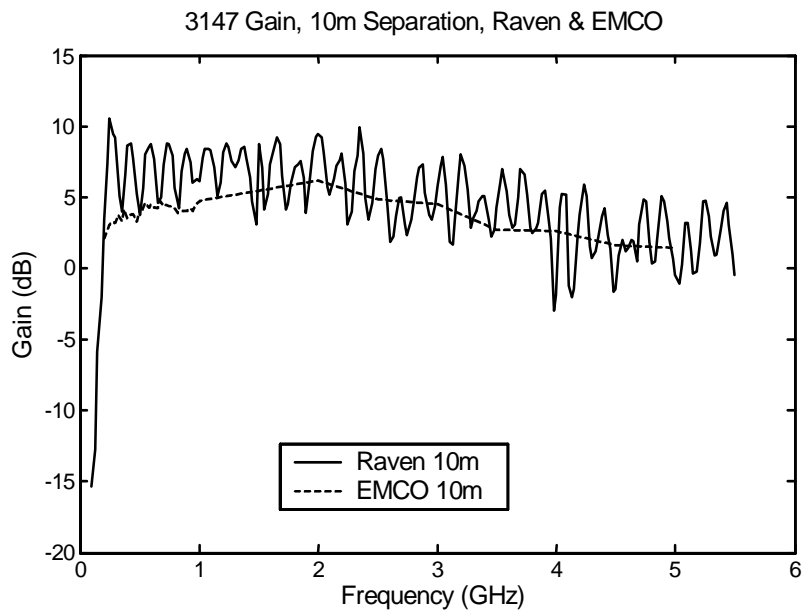
Figure 5.7. Raven measurement and EMCO calibration data at 10-meter separation.
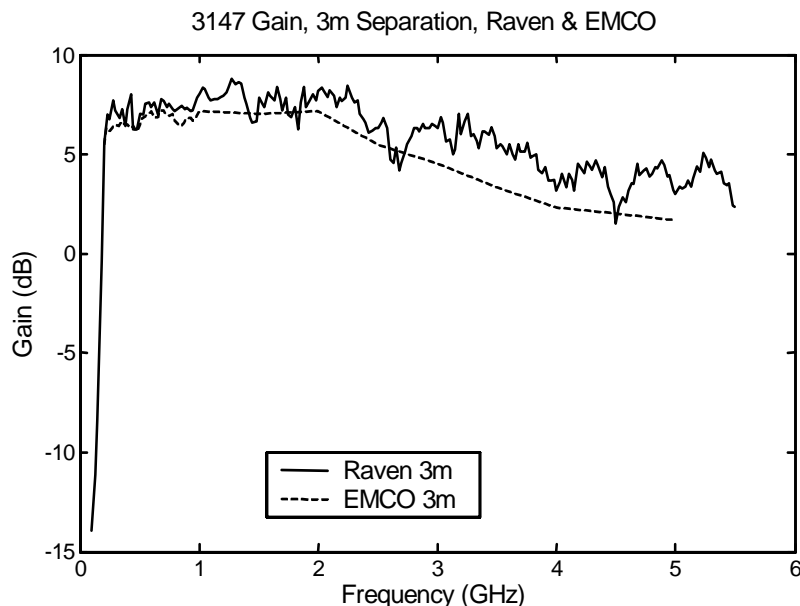
Figure 5.8. Raven measurement and EMCO calibration data at 3-meter separation.

D. Conclusions on the EMCO 3147 Measurements

We were unable to characterize satisfactorily the EMCO 3147 log-periodic dipole array with our time domain antenna range. This may have been due to either the long time window, the ground bounce, or a combination of the two. We note that ground bounce was not a problem in the Raven measurements made at 3-meter distance. This is a bit puzzling to us, because at 3 meters we observed oscillations at periodic frequencies corresponding to the time delay between the direct and ground-bounce ray. It is possible that Raven had a ground that was less reflective than ours, but that seems unlikely to explain all differences.

We tested the 3147 using a second source, the PSPL 2000D, to see if we could improve our low-end frequency response. We found no improvement with the 2000D, however, we found a degradation of the high-end response. So the PSPL 4015C was a better overall choice.

VI. Return Loss Measurements of Printed Circuit Board Log-Periodic Dipole Arrays

   To evaluate the accuracy of our measurements of return loss, or S_{11}, we measured the S_{11} of two small printed circuit board (PCB) dipole antennas and two small PCB log periodic dipole arrays. These were then compared to frequency domain measurements made with a vector network analyzer, an Agilent 8720ES. Pictures of the antennas are provided in Figures 6.1, and the data are all shown in Figures 6.2 and 6.3, where, for each antenna, we compare the time domain and VNA determinations of S_{11}. We obtained excellent agreement on S_{11} measurements between measurements made with the time domain and frequency domain methods.

(a) PCB LPDA with thin dipole elements   (b) PCB LPDA with wide dipole elements

(c) PCB thin-element dipole   (d) PCB wide-element dipole

Figure 6.1 PCB Antennas

Figure 6.2. S_{11} for a wide dipole (left) and a narrow dipole (right).
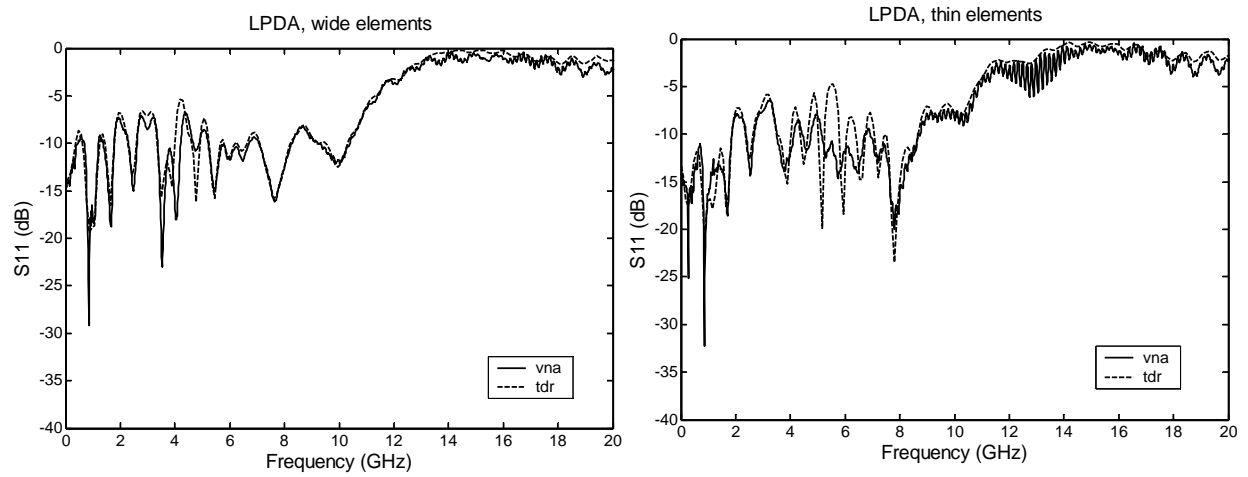
Figure 6.3. S_{11} for a log-periodic antenna with wide elements (left) and with thin elements (right).

We also measured the gain of these antennas, however, we do not have anything to compare their response against in the frequency domain. The data may nevertheless be interesting in order to demonstrate that resonant devices may be measured on our antenna range as low as 1 GHz. The gain of the dipoles is provided in Figure 6.4, and that of the LPDAs are provided in Figure 6.5.
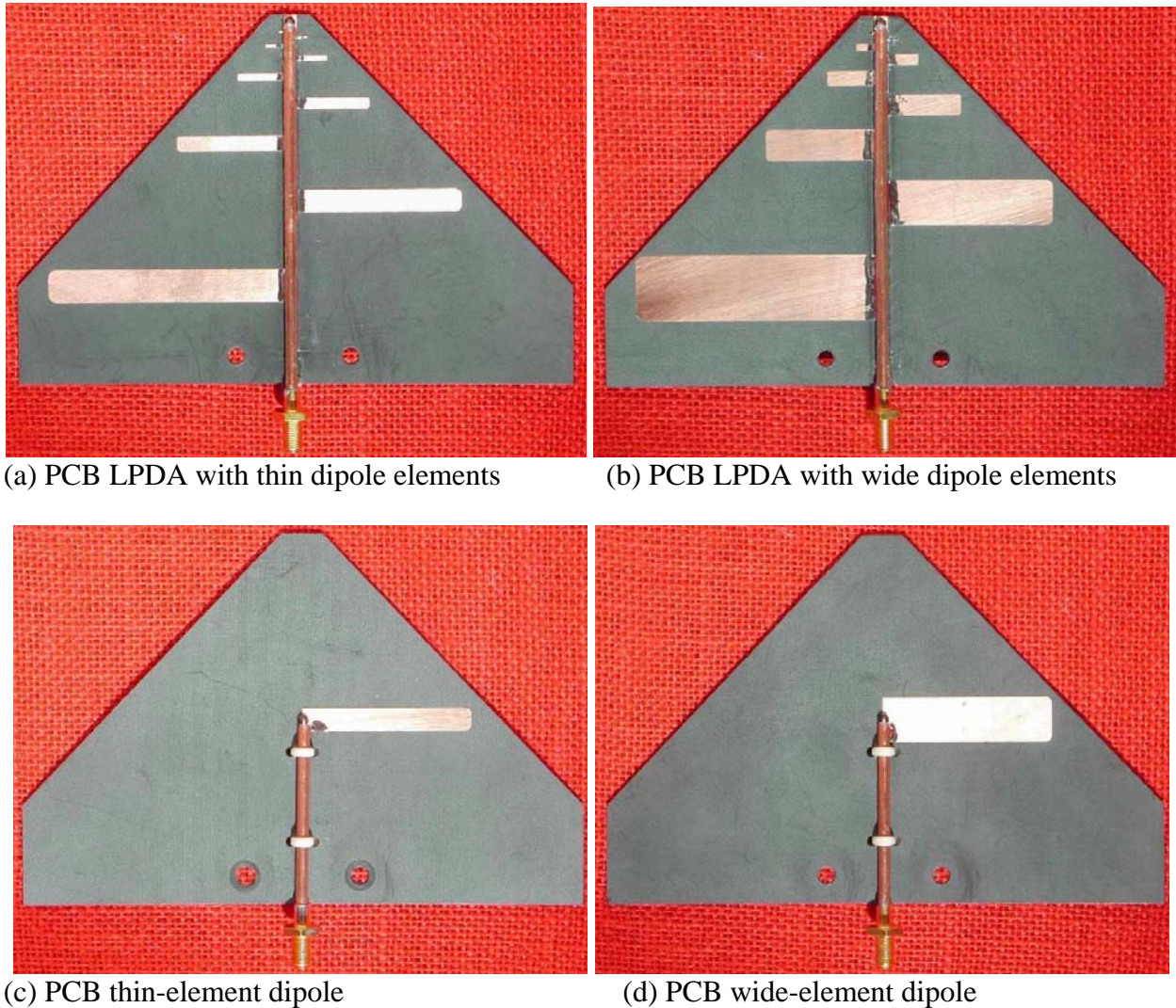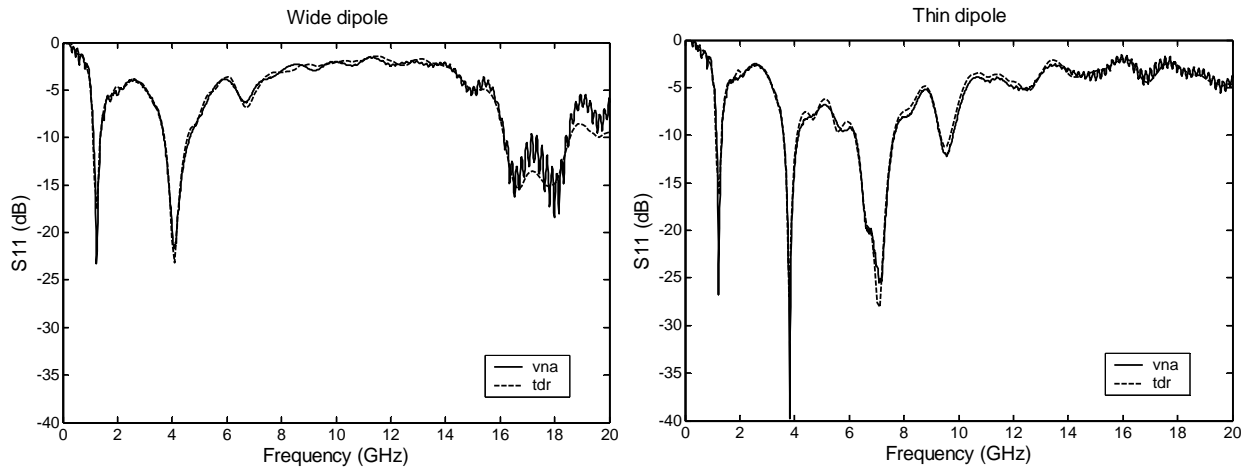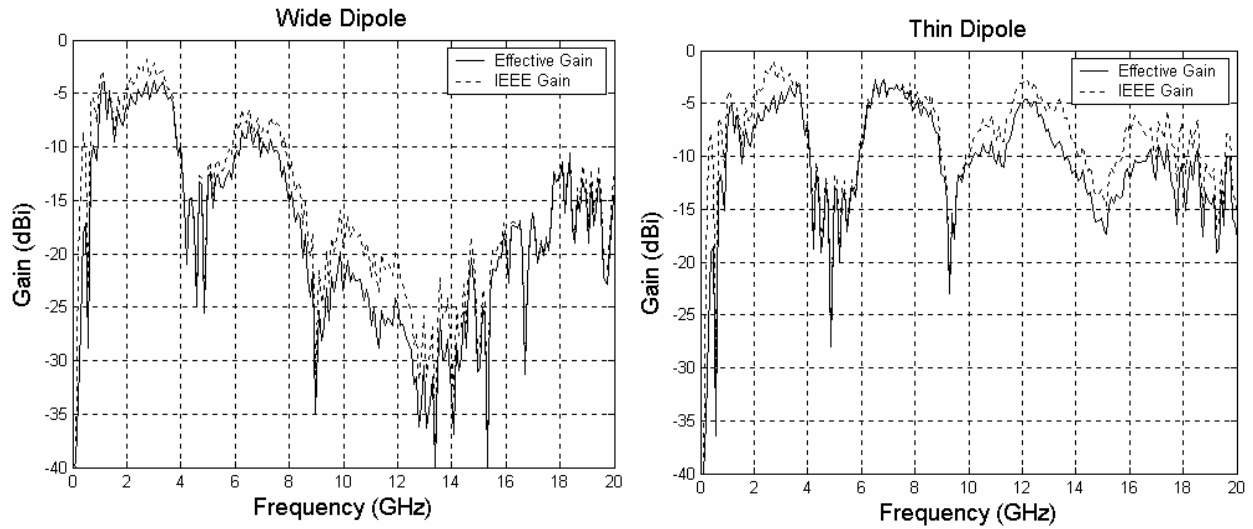

Figure 6.4. Gain for a wide dipole (left) and a narrow dipole (right).
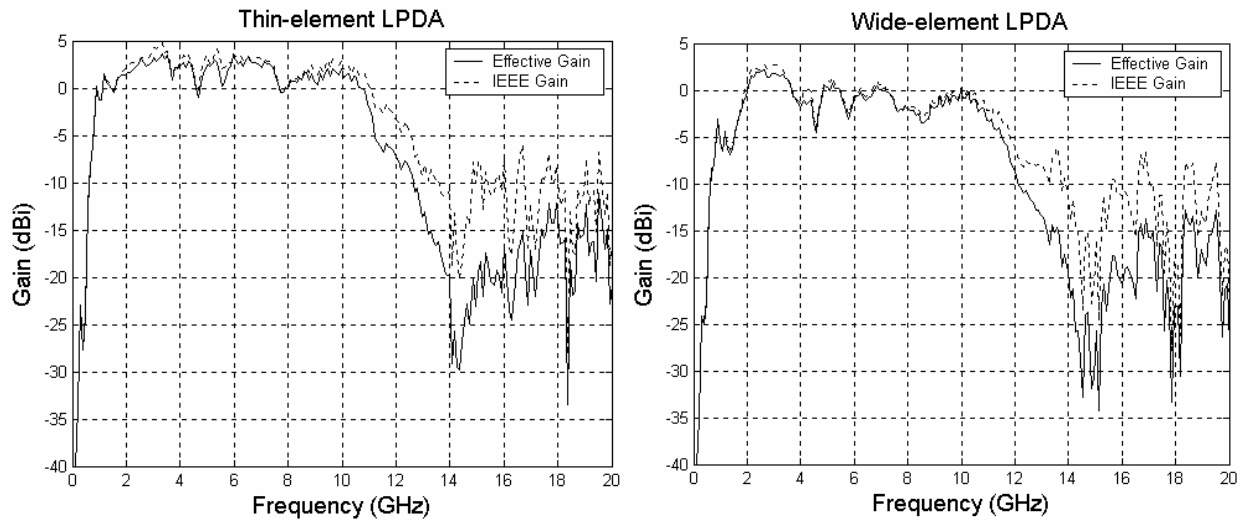
Figure 6.5. Gain for a log-periodic antenna with wide elements (left) and with thin elements (right).

VII. Measurements of Yagi and Folded Dipole Antennas

To study the antenna range performance at frequencies below 1 GHz, we selected three resonant antennas: two Cushcraft Yagis (Models A449-6S and 224WB) and an M^2 folded dipole (Model 900-930-6W). The antennas are shown in Figure 7.1, and a table of their characteristics is provided in Table 7.1. For these antennas, we only have limited manufacturer descriptions on these antennas, instead of the independent measurements or calibrations that we would prefer. Nevertheless, studying these antennas can still give us a feel for the low-frequency capabilities of our time domain antenna range.

Figure 7.1. Test antennas – from top to bottom: Cushcraft A4496S (6-element yagi), M^2 Model 900-930-6W (6-element folded dipole), and Cushcraft 224WB (4-element Yagi).

Table 7.1. Resonant Antennas

Manufacturer	M^2	Cushcraft	Cushcraft
Model	900-930-6W	A449-6S	224WB
Type	Folded Dipole	Yagi, 6-element	Yagi, 4-element
Frequency range (MHz)	900-930	440-450	220-225
Gain over dipole (dBd)	10.1	10.5	10.2
Gain over isotropic (dBi)	12.3	12.7	12.4
Front to back ratio (dB)	16	18	24
Impedance (ohms)	50	50	50
3 dB Beamwidth E-plane (degrees)	48	60	60
3 dB Beamwidth H-plane (degrees)	56	Not listed	83
Longest element (cm)	16	68	33

A. Testing and the Analysis Time Window

We begin by observing that analysis of the normal ring-down of a deliberately resonant antenna may be strongly affected by our choice of a time window. In Figures 7.2 and 7.3, we show the impact on gain of a folded dipole for two possible time window choices. In the first instance, we retain only the first few cycles of the ring-down; in the second, we retain an essentially complete ring-down. The gain in this second figure is close to 12.3-dBi specification for the M^2 folded dipole. These two figures demonstrate that it is necessary to retain the complete time record to get accurate results.

Windowed Folded Dipole Data

Effective Antenna Gain on Boresight (dBi)
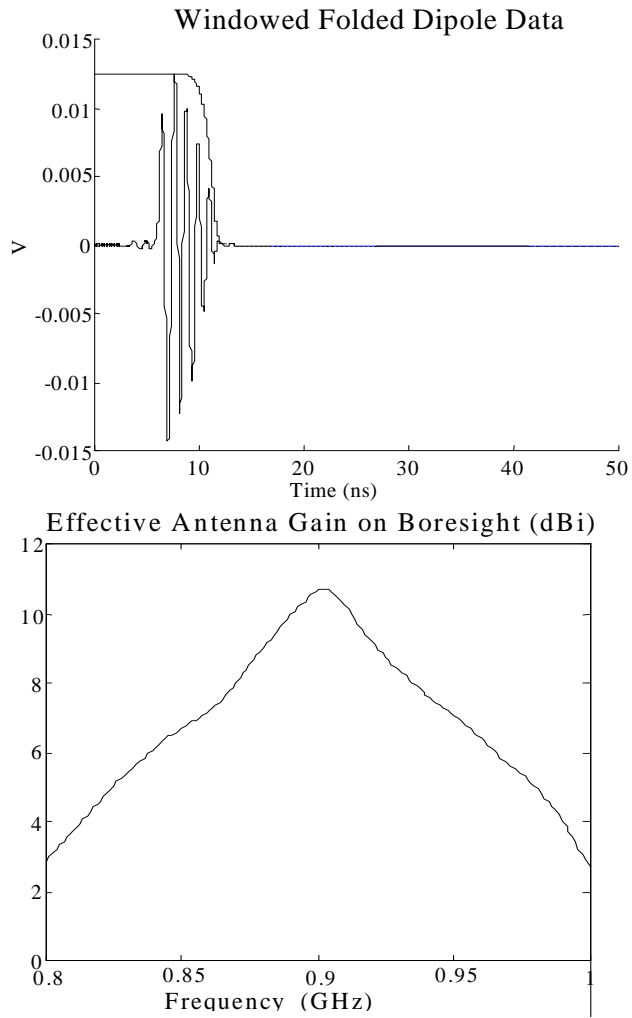
Figure 7.2. Gain of M^2 folded dipole from truncated time domain data.

Windowed Folded Dipole Data

Effective Antenna Gain on Boresight (dBi)
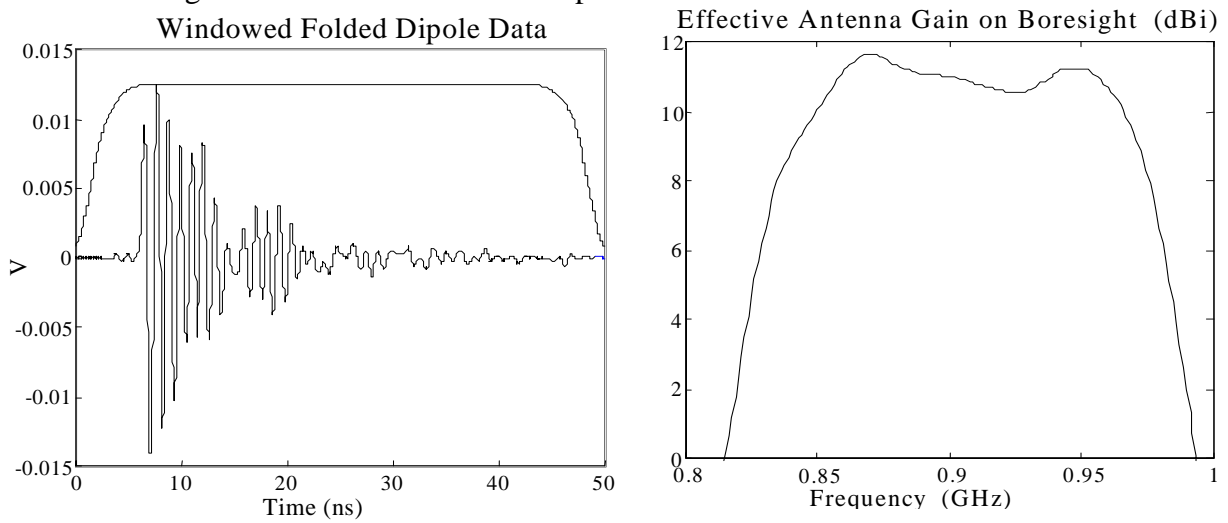
Figure 7.3. Gain of folded dipole from complete time domain data.

26

B. Gain Measurements

We measured the gain of all three antennas and present the data in Figures 7.4 through 7.7. In each figure we present the raw data, the time domain impulse response and the gain plotted on both logarithmic and linear frequency scales.

We acquired all data on our time domain antenna range using the PSPL Model 2000D pulse generator configured for a 50-ns wide pulse. The antennas were separated by approximately ten meters, and were supported three meters above the earth.

Figure 7.4 shows the data for the M^2 900-930-6W folded dipole. We acquired this data with a 50-ns time window. Note that the complete waveform is captured.

(a). Raw data.

(b). Impulse Response

(c). Antenna gain on log scale.

(d). Antenna gain on linear scale.
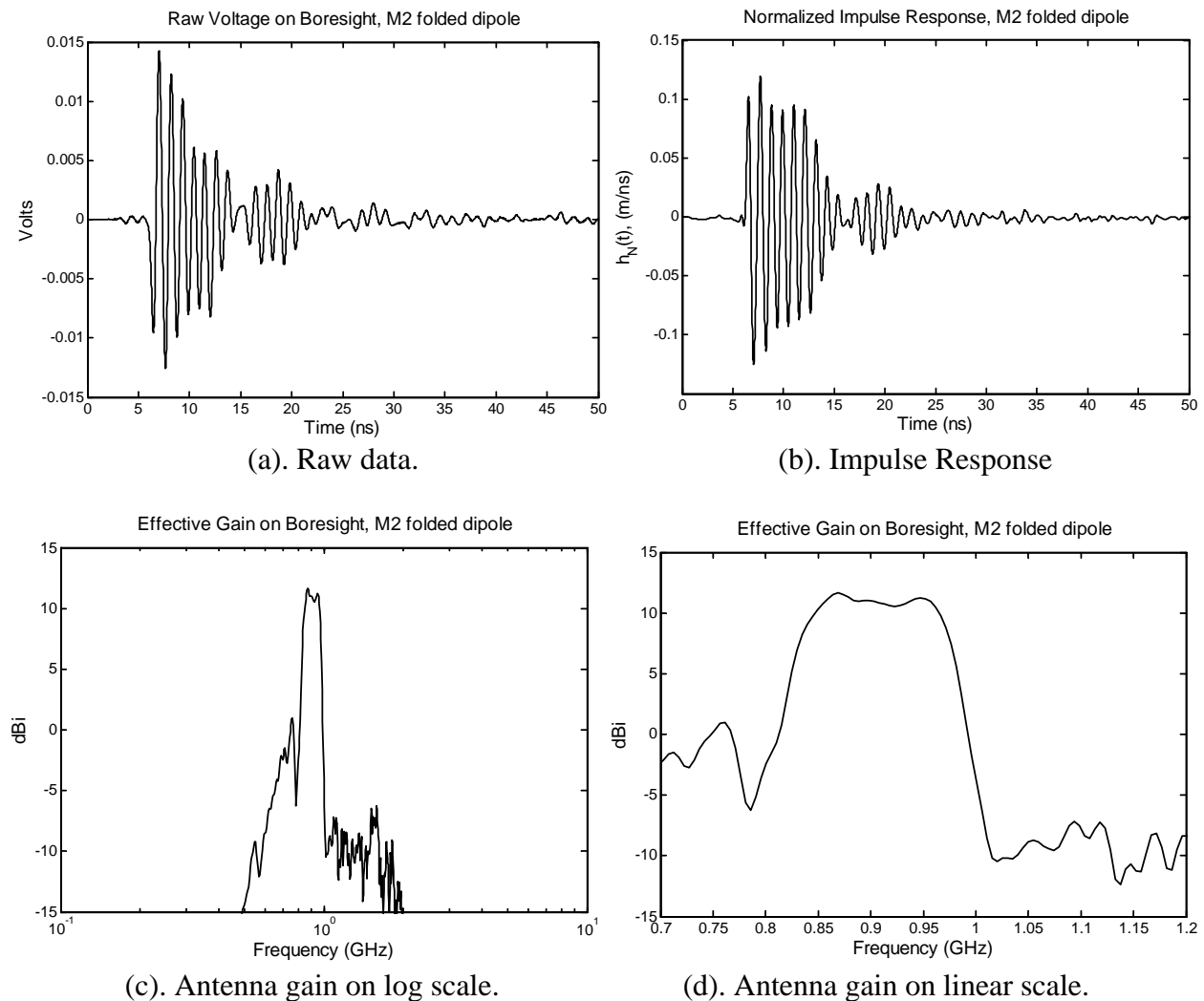
Figure 7.4. Results for the M^2 Model 900-930-6W (6-element folded dipole)

The measured peak of the M^2 900-930-6W is 11.6 dBi. M^2 specifies the gain as 12.3 dBi. The measured 3dB bandwidth is 840 to 970 GHz compared to M^2's specification of 900 to 930 MHz *usable* bandwidth. M^2 did not specify exactly what they meant by *usable bandwidth* in telephone conversation. Despite the sketchy reference data, we believe that this antenna was well characterized by our system.

Next, we provide the data for the Cushcraft A449-6S Yagi in Figure 7.5. First, we acquired this data with a 50 ns time window. Note that the waveform is *not* completely captured.

(a) Raw data.

(b) Impulse Response

(c) Antenna gain on log scale.

(d) Antenna gain on linear scale.

Figure 7.5. Cushcraft A449-6S (6-element yagi)

The measured gain for this set of data is only 9.4 dBi compared to the Cushcraft specification of 12.7 dBi. We repeated this measurement, as shown in the next set of data, but doubled the acquisition window to 100 ns.

Figure 7.6 is a second set of data for the Cushcraft A449-6S Yagi. We acquired this data with a 100 ns time window. Note that the waveform is more complete than the waveform of the data in Figure 7.5, but the waveform is still not completely captured. The more complete waveform results in a higher gain and more data structure.

(a). Raw data.

(b).Impulse Response

(c). Antenna gain on log scale.

(d). Antenna gain on linear scale.

Figure 7.6. Cushcraft A449-6S (6-element Yagi)

The measured peak of the Cushcraft A449-6S is 13.3 dBi. Cushcraft specifies the gain as 12.7 dBi. The measured 3dB bandwidth is 445 MHz to 452 MHz compared to Cushcraft's specified frequency range of 440 to 450 MHz. Note that Cushcraft also specifies a generic frequency range, which is not necessarily the 3 dB bandwidth. We believe that the quality of this measurement is marginal, but it might be possible to improve this measurement by increasing the time window.

Finally we provide the data for the Cushcraft 224WB Yagi in Figure 7.7. We acquired this data with a 100 ns time window. Note that the waveform is *not* completely captured.
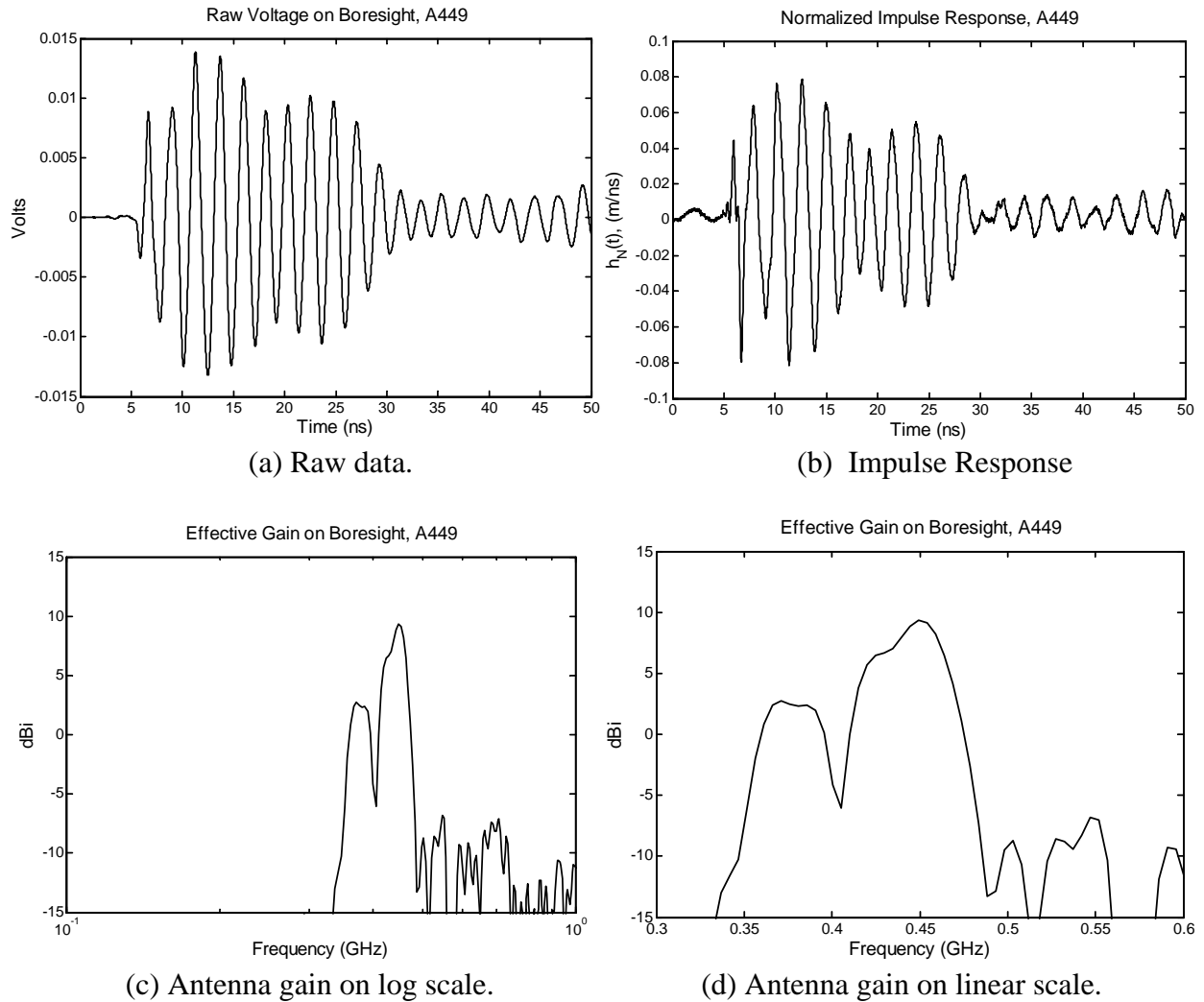

(a) Raw data.

(b).Impulse Response

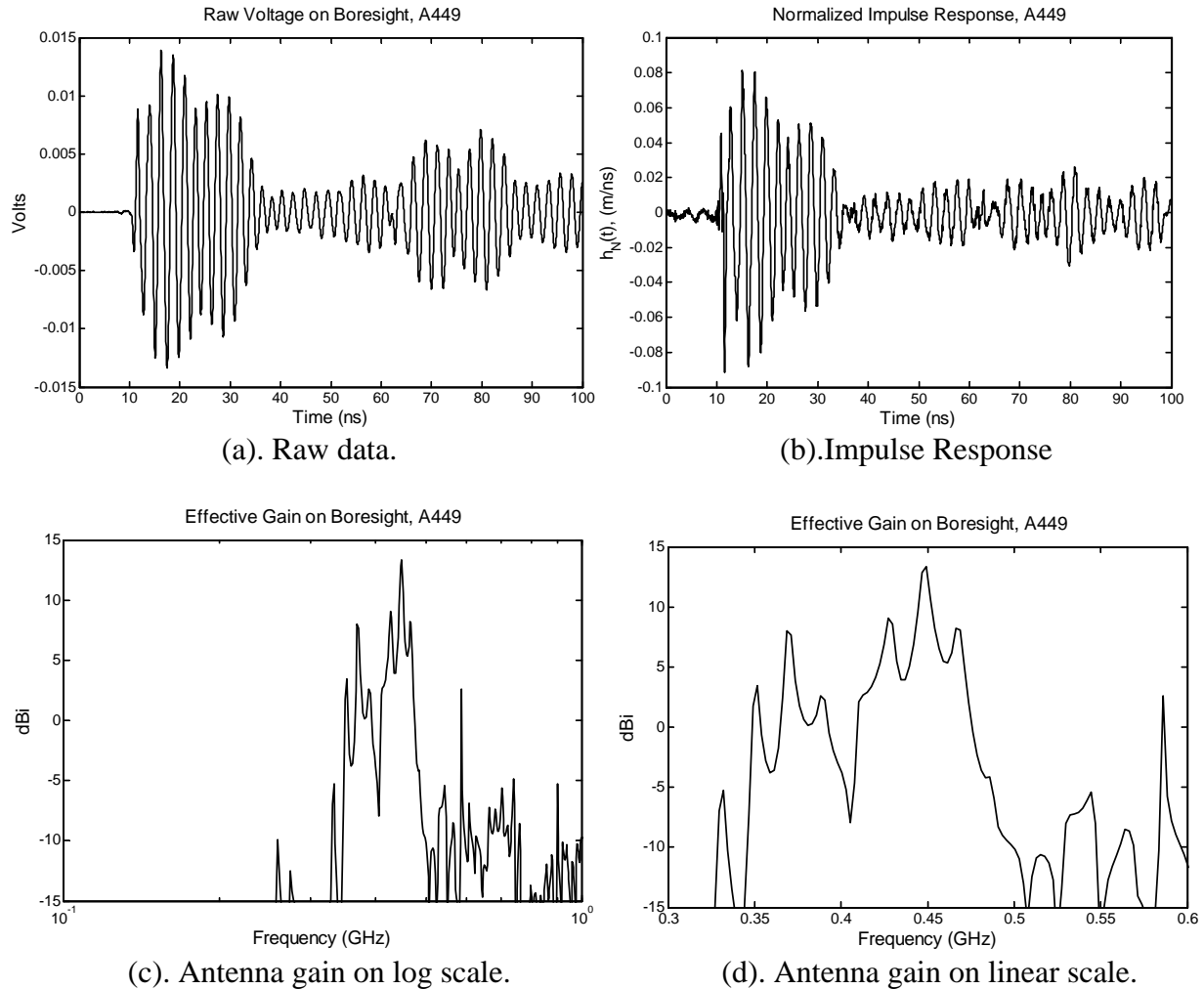(c) Antenna gain on log scale.

(d). Antenna gain on linear scale.
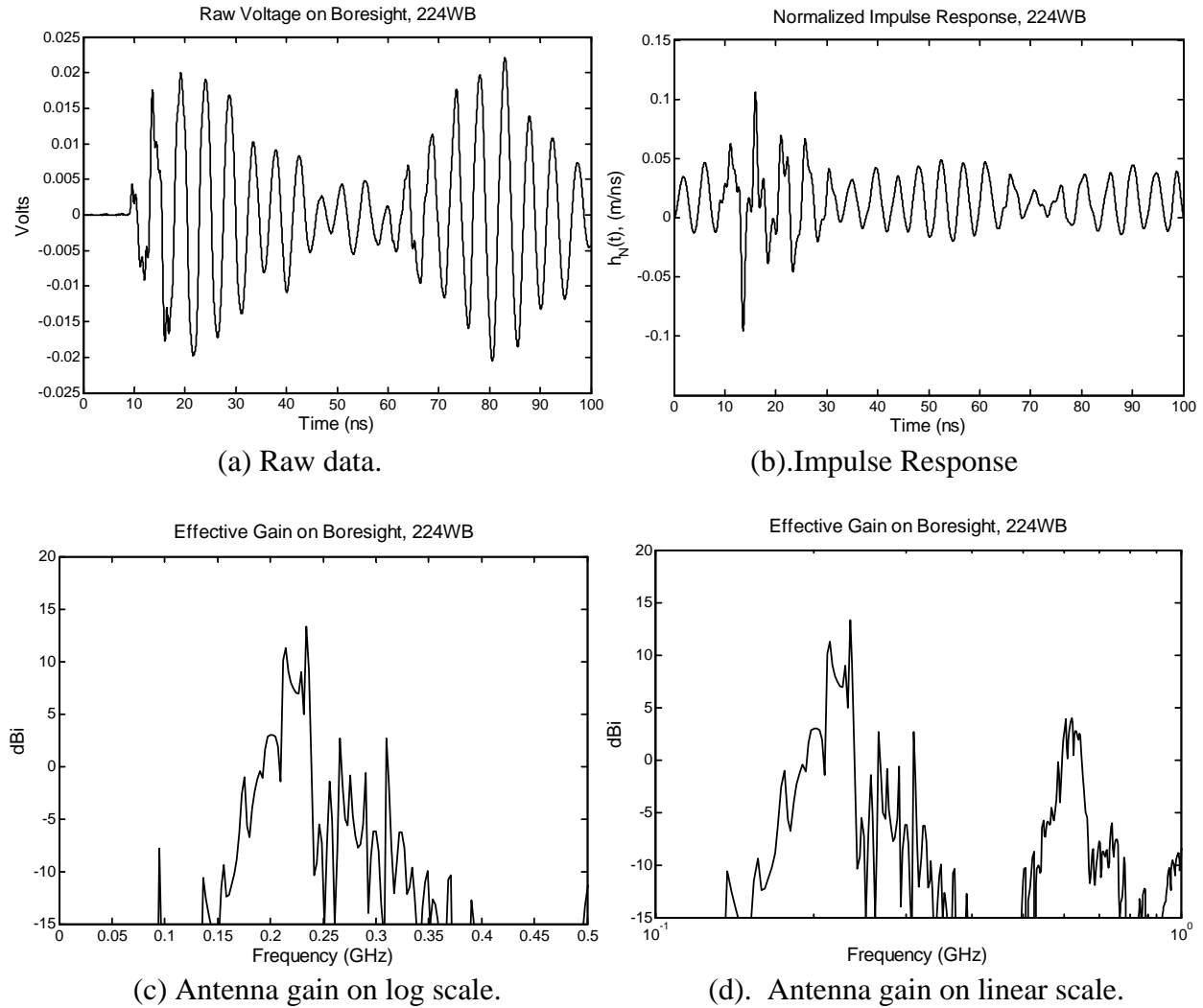
Figure 7.7. Cushcraft 224WB (6-element yagi)

The measured peak of the Cushcraft 224WB is 13.3 dBi. Cushcraft specifies the gain as 12.4 dBi. The measured 3dB bandwidth is 233 MHz to 236 MHz, compared to the frequency range specified by Cushcraft: 222 to 225 MHz. We would characterize this measurement as inadequate, however a longer time window might have improved the result.

For these three antennas, we have measured the peak gain to within 1 dB of the manufacturer's specification, even when we have an incomplete time record. It is not so clear that we have good agreement with the bandwidth because we do not have a clear definition of bandwidth from the manufacturer. From these three antenna measurements we can conclude that low-frequency resonant antenna measurements may be feasible. Long antenna ring-downs become problematic due to clear times, ground bounce, and pulse generator output structure. Changes in data truncation within the data-processing program lead to varying gain outputs.

C. S_{11} Measurements

We measured the S_{11} of the Cushcraft Model A449-6S, 450-MHz Yagi, and compared it to frequency domain measurements. We recorded the TDR with our Tektronix TDS8000 oscilloscope and 80E04 sampling head, processing the data by simply Fourier transforming its derivative to obtain the S_{11} approximation. Note that for a rigorous measurement, a deconvolution is normally implemented, but at low frequencies we thought that to be to be unnecessary. For the frequency domain comparison, we recorded the S_{11} of the antenna using a Hewlett Packard model 8720ES vector network analyzer. The S_{11} overlays of the two techniques are shown below in Figure 7.8. We observe good agreement between the two methods.

S11, Cushcraft A449-6S Yagi (440-450MHz)
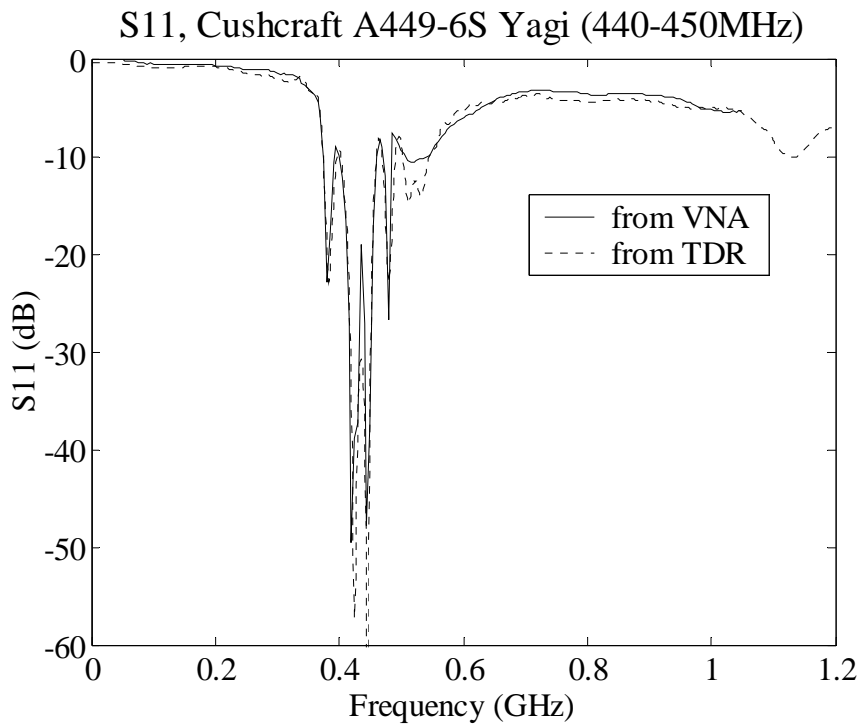
Figure 7.8. Cushcraft A449 Yagi S_{11} comparison.

VIII. Measurements of a Narda 640 Standard Gain Horn

Next, we measured the gain of a Narda Model 640 X-band standard gain horn, as shown in Figure 8.1. This was of particular interest to us, because a horn is not intended to be driven by an impulse-like waveform. The gain was measured at an antenna separation of 4.15 meters.

Figure 8.1. Narda X-band horn.

First, we show in Figure 8.2 the raw voltage on boresight and the corresponding normalized impulse response. We note that the signal resonates only for about 2 nanoseconds, so it is relatively easy to capture the entire waveform.
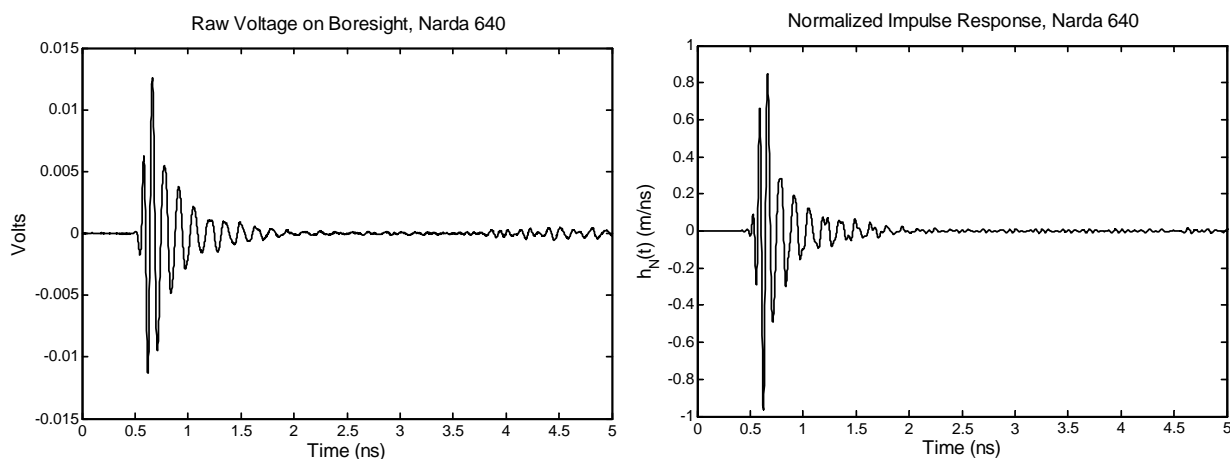
Figure8.2. Raw voltage (left), and normalized impulse response (right) for the Narda 640 horn.

Next, we measured the boresight gain. Narda specifies the horn to have a gain that increases monotonically in an approximately linear fashion over the frequency range of the horn. We have plotted Narda's typical gain in Figure 8.3, along with our measured data. We observe that our measured data is well within 1 dB of the Narda's typical data, which we consider to be

outstanding agreement. We also show the effective gain in Figure 8.3. There is little difference between effective gain and gain, as we would expect for a well-matched antenna.

Gain on Boresight, Narda 640
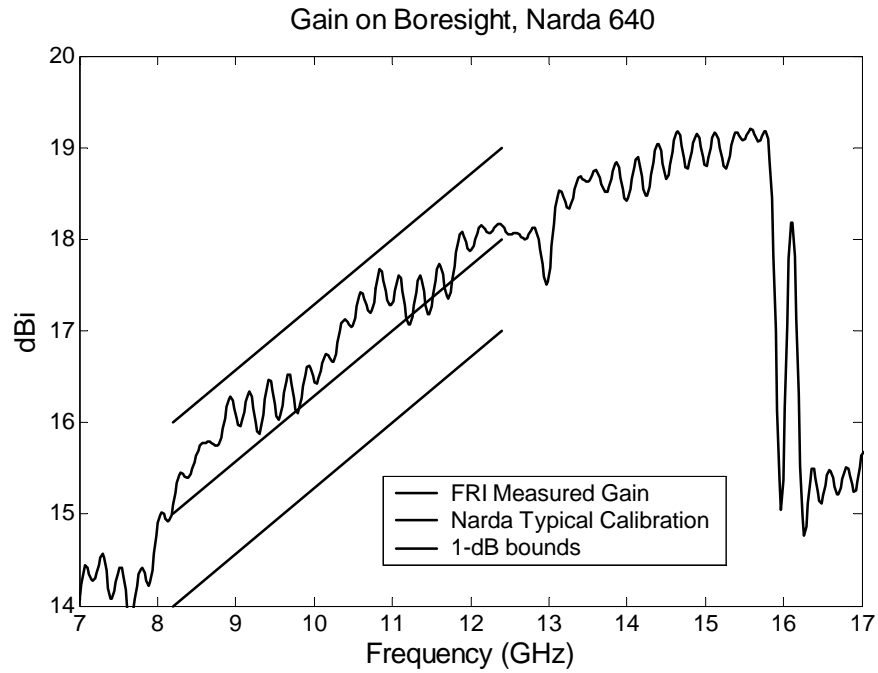
Figure 8.3. Narda 640 IEEE Gain, typical specifications and our measurements.

Effective Gain on Boresight, Narda 640
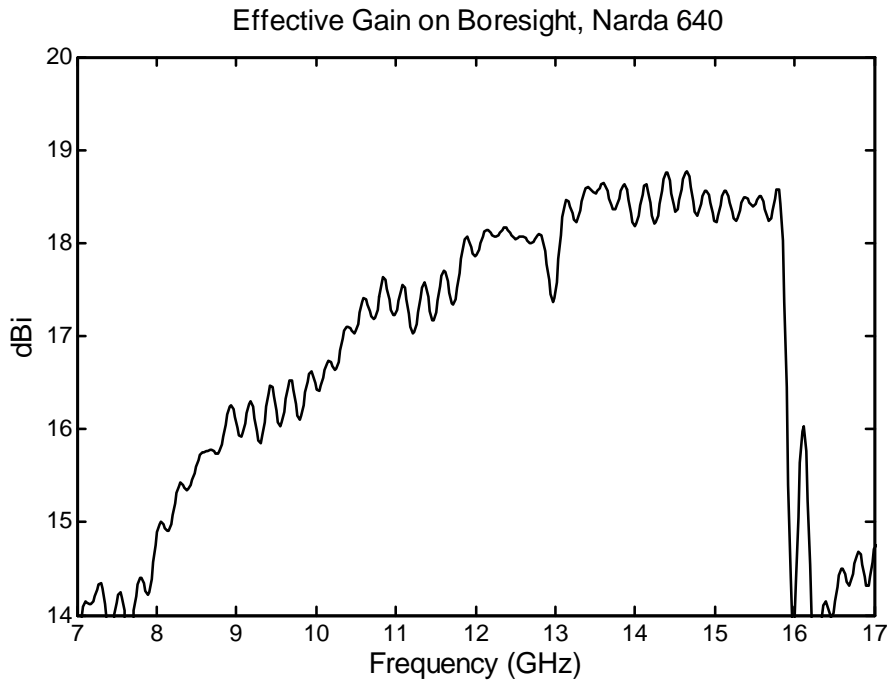
Figure 8.4. Narda 640 Effective Gain as measured on our range.

IX. Discussion

The antenna range we have developed is well suited to measuring IRAs over a range of 200 MHz to 20 GHz. It also characterized well the EMCO 3115 double-ridged waveguide horn over a range of 1-18 GHz. Both antennas radiate waveforms that are well damped, so it is easy to capture their characteristics within a short time window.

Our system appears not to be well suited for characterizing the EMCO 3147 log-periodic dipole array, operating from 200 MHz to 5 GHz. This is probably due in part to the antenna's highly resonant nature, which requires a very long time window. It may also be due in part to the ground bounce that must be included in long time windows. This remains a bit of a puzzle to us, because the outdoor Raven frequency domain measurements at 3-meter range and 3-meter height were reasonable.

Our measurements of S_{11} are quite good, based on the measurements of the printed-circuit LPDA (1-12 GHz). So we are comfortable expressing antenna performance in terms of either gain or effective gain. It remains our conviction that effective gain is the more useful measure of antenna performance for UWB applications, because it includes mismatch loss. But we concede that most applications require simple gain, so it is necessary to characterize antennas both ways.

Our measurements of the M^2 model 900-930-6W folded dipole, which operates at 900-930 MHz, were quite reasonable. This gives us some assurance that even resonant antennas can be measured on our antenna range as low as 900 MHz. This helps to simplify our specification to "any antenna above 900 MHz." The measurements of the two Cushcraft Yagis suggest that measurements of resonant antennas at 450 MHz and below are less precise, but even these might have been improved by using a longer time window.

Our measurements of the Narda 640 X-band pyramidal horn were in excellent agreement with manufacturer's specifications. This is significant because an X-band horn is a highly resonant structure, and it was never intended to be driven by an impulse.

When making measurements at lower frequencies, it is important to capture the entire waveform. We had thought that we might get the high-frequency information on an antenna by capturing just the early-time data, but that did not prove to be successful. To get this to work, it may be possible to fit a sum of damped sines to the early-time data, in order to get a complete waveform, thereby allowing one to extrapolate out to late times. This process, sometimes referred to as "Model Based Parameter Estimation," was not investigated in this effort, but it may be useful to investigate in future studies.

We had hoped that using a source with a higher voltage and slower risetime would improve the low-end accuracy of our measurement. However, we never observed that effect in our measurements. The only effect observed was the expected degradation of the high-end performance due to the slower risetime. It is possible that using a slower source would have worked better if we had placed our antennas higher than three meters above ground, but 3 meters seemed to be the highest we could operate conveniently.

X. Conclusions

Our time domain antenna range has demonstrated the ability to characterize all antennas that operate between 900 MHz and 20 GHz. For non-resonant antennas, such as IRAs, we obtain good results as low as 200 MHz. It may be possible to push the frequency range for resonant antennas even lower than 900 MHz by using a larger time window. This may also require us to position our antennas higher than three meters above ground.

It is hoped that a time domain antenna measurement system similar to this will become a useful commercial product. This system has allowed us to quickly characterize and tune our antennas without incurring the expense and delay required to send them away to a separate measurement facility. This system is significantly less expensive than comparable frequency domain systems. Our system is also deployable and portable, so a dedicated facility is not required. Having a system in-house that is simple, accurate, and low cost should allow many to develop their own antennas who might otherwise find the process too cumbersome.

Acknowledgements

References

1. W. S. Bigelow, E. G. Farr, L. H. Bowen, T. C. Tran, C. E. Baum, and W. D. Prather, Automated Time Domain Antenna Range Initial Implementation, Sensor and Simulation Note 456, May 2001.

2. IEEE, *IEEE Standard* Definition *of Terms for Antennas*, IEEE Std 145-1993, Institute for Electrical and Electronics Engineering, Inc., New York, March 1993.

3. E. G. Farr and C. E. Baum, Time Domain Characterization of Antennas with TEM Feeds, Sensor and Simulation Note 426, October 1998.

4. L. H. Bowen, E. G. Farr, and W. D. Prather, "A Collapsible Impulse Radiating Antenna," *Ultra-Wideband, Short-Pulse Electromagnetics 5*, Kluwer Academic Press, 2002, pp. 299-309. Also presented at the 2000 EUROEM conference in Edinburgh.

5. George H. Hagn, Personal communication, January 2000.

Appendix A: Antenna Equations and Definitions

In Appendices A-D, we provide all the equations used to process the data associated with our time domain antenna range.

Basic Equations

We find it useful to carefully define the antenna equations and definitions used in this paper, because the time domain description of antennas is not yet treated well in the IEEE standard for antenna definitions [2]. We have defined a single waveform, $h_N(t)$, which describes an antenna's performance in both transmission and reception. This quantity is the normalized impulse response in reception and the normalized step response in transmission. For convenience, we simply refer to this as the antenna impulse response.

We have found that the antenna equations exhibit a striking simplicity and symmetry if they are expressed not in terms of electric fields and voltages, but in terms of square-root of power or power density. Thus, instead of voltages we use voltages divided by the square root of the cable impedance; and instead of electric fields, we use electric fields divided by the square root of the intrinsic impedance of free space. In this format, we have the reception and transmission equations as [3]

$$\frac{V_{rec}(t)}{\sqrt{50\,\Omega}} = h_N(t) \circ \frac{E_{inc}(t)}{\sqrt{377\,\Omega}}$$

$$\frac{E_{rad}(t)}{\sqrt{377\,\Omega}} = \frac{1}{2\pi c r} h_N(t) \circ \frac{d V_{src}(t)/dt}{\sqrt{50\,\Omega}}$$

(A.1)

where $V_{rec}(t)$ is the received voltage into a 50-ohm load or oscilloscope, and $V_{src}(t)$ is the source voltage as measured into a 50-ohm load or oscilloscope. Furthermore, $E_{inc}(t)$ is the incident electric field, $E_{rad}(t)$ is the radiated electric field, r is the distance away from the antenna, c is the speed of light in free space, and "$\circ$" is the convolution operator. Note that the above expressions refer by default to the dominant polarization on boresight, but they are easily extended to multiple angles and polarizations. Note also that $h_N(t)$ has units of meters per second.

The above expressions have a number of advantages over earlier formulations, such as the expressions presented in the first half of [3]. First, all the voltages are those measured into an oscilloscope with 50-ohm impedance, so it is simple to measure all these quantities. Second, the equations are in the simplest possible form. Third, there is no need to define transmission coefficients or the characteristic impedance of antennas. In our opinion, these add an unneeded ambiguity and complexity to the equations.

A simpler version of the above equations can be used with some Ultra-Wideband antennas if $h_N(t)$ can be approximated as an impulse with area h_{Na}, or $h_N(t) \approx h_{Na}\, \delta(t)$. With this approximation, the equations simplify to

$$\frac{V_{rec}(t)}{\sqrt{50\,\Omega}} \approx h_{Na} \frac{E_{inc}(t)}{\sqrt{377\,\Omega}}$$

$$\frac{E_{rad}(t)}{\sqrt{377\,\Omega}} \approx \frac{h_{Na}}{2\pi c r} \frac{dV_{src}(t)/dt}{\sqrt{50\,\Omega}} \tag{A.2}$$

$$h_{Na} = \int_{Impulse} h_N(t)\,dt$$

When we calculate h_{Na} from experimental data, it is usually not clear how much of the waveform should be included in the above integral. Such subjective decisions can lead to significant differences in the calculation of h_{Na}, so one should understand the approximation in this light. Note that this approximation is appropriate only at mid-band – it obviously fails both at dc and very high frequencies. Note also that this approximation is most useful for those antennas, such as the Farr Research TEM sensors, whose impulse response is shaped most like an impulse. The impulse area, h_{Na} , could be expressed alternatively in terms of the effective height of the antenna as

$$V_{rec}(t) \approx h_{eff}\,E_{inc}(t)$$

$$h_{eff} = \sqrt{\frac{50\,\Omega}{377\,\Omega}}\,h_{Na} = \frac{h_{Na}}{2.75} \tag{A.3}$$

Both h_{Na} and h_{eff} have units of meters.

Two-Antenna Equations

We now consider the case when we have both a transmitting and receiving antenna. In this case, we can relate the received voltage to the source voltage by combining the two equations in (A.1) as

$$V_{rec}(t) = \frac{1}{2\pi rc}\,h_{N,RX}(t) \circ h_{N,TX}(t) \circ \frac{dV_{src}(t)}{dt} \tag{A.4}$$

where $h_{N,RX}(t)$ is the normalized impulse response of the receive antenna and $h_{N,TX}(t)$ is the corresponding response of the transmit antenna.

To calibrate our measurement system, we use two identical TEM sensors. In this case, the combined antenna equation becomes

$$V_{rec}(t) = \frac{1}{2\pi rc}\,h_{N,tem}(t) \circ h_{N,tem}(t) \circ \frac{dV_{src}(t)}{dt} \tag{A.5}$$

The normalized frequency domain impulse response of the sensors can be extracted from (A.5) as

$$\tilde{h}_{N,tem}(\omega) = \sqrt{\frac{2\pi rc \tilde{V}_{rec}(\omega)}{j\omega \, \tilde{V}_{src}(\omega)}} \qquad (A.6)$$

We normally account for the factor of $j\omega$ by taking the Fourier transform of the derivative of the source voltage. We can measure the response of an antenna under test (AUT) by replacing one of the sensors with the antenna under test. The impulse response of the antenna then becomes

$$\tilde{h}_{N,AUT}(\omega) = \frac{2\pi rc \tilde{V}_{rec}(\omega)}{j\omega \, \tilde{V}_{src}(\omega) \, \tilde{h}_{N,tem}(\omega)} \qquad (A.7)$$

and the time domain normalized impulse response is found with an inverse Fourier transform. A number of details are important regarding the deconvolution and complex square-root, and these are treated in Appendix D.

Related Parameters: Gain, Effective Gain and Antenna Factor

Next, we convert the normalized impulse response to effective gain, gain, and antenna factor. Here we merely cite the final result, but the derivations are provided in Appendix B. First, effective gain is expressed as [4]

$$G_{eff}(\omega) = \frac{4\pi}{\lambda^2} |\tilde{h}_N(\omega)|^2 = \frac{4\pi f^2}{c^2} |\tilde{h}_N(\omega)|^2 \qquad (A.8)$$

For those cases where a UWB antenna's time domain impulse response is approximated by a delta function, $h_N(t) \approx h_{Na} \, \delta(t)$, then $|h_N(\omega)| \approx h_{Na}$, and the effective gain is approximately

$$G_{eff}(\omega) \approx \frac{4\pi h_{Na}^2}{\lambda^2} = \frac{4\pi f^2 h_{Na}^2}{c^2} \qquad (A.9)$$

which is valid only at mid-band. The relationship between effective gain and the standard definition of gain used by IEEE [2] is

$$G_{eff}(\omega) = G(\omega)\left[1 - |S_{11}|^2\right] \qquad (A.10)$$

where S_{11} is the standard scattering parameter looking into the antenna port as measured in a 50-ohm system. Effective gain is sometimes a more useful measure of antenna performance than gain, because it includes impedance mismatch. It also simplifies the signal processing on a time domain antenna range, because a measurement of S_{11} is not required. Note that for well-matched antennas, the two versions of gain are very close.

Finally, antenna factor is expressed as

$$AF = \frac{\tilde{E}_{inc}(\omega)}{\tilde{V}_{rec}(\omega)} = \sqrt{\frac{377}{50}} \frac{1}{\left|\tilde{h}_N(\omega)\right|} = \frac{9.73}{\lambda\sqrt{G_{eff}}} \qquad (A.11)$$

As before, note that $|\tilde{h}_N(\omega)|$ may be approximated as h_{Na} at midband.

Appendix B: Derivation of the Expressions for Gain, Effective Gain, and Antenna Factor

We clarify here the origin of equations (A.8) through (A.11), which define the gain, effective gain, and antenna factor.

Gain and Effective Gain

To derive our expression for effective gain, we begin with the standard expressions in the frequency domain. Thus, the power received into a 50-ohm feed cable is

$$P_{rec} \;=\; \varepsilon\, A_{eff}\; S_{inc} \tag{B.1}$$

where S_{inc} is the incident power density in W/m^2, A_{eff} is the effective aperture, and ε is a power transmission coefficient that accounts for the impedance mismatch between the antenna port and 50-ohm feed cable. Absolute gain is related to effective aperture by

$$A_{eff} \;=\; \frac{\lambda^2}{4\,\pi}G \;=\; \frac{\lambda^2}{4\,\pi}\frac{G_{eff}}{\varepsilon} \tag{B.2}$$

where G_{eff} is the effective gain, the gain after accounting for the impedance mismatch between the antenna port and the 50-ohm feed cable. The term "effective gain" has not yet been recognized by the IEEE Std. 145 [2], but it is in common use[5]. Combining the above two equations, we have

$$P_{rec} \;=\; \frac{\lambda^2\, G_{eff}}{4\,\pi}S_{inc} \tag{B.3}$$

By taking the square root of this equation, and recasting into voltages, we find

$$\frac{\tilde{V}_{rec}(\omega)}{\sqrt{50\,\Omega}} \;=\; \frac{\lambda\,\sqrt{G_{eff}(\omega)}}{2\sqrt{\pi}}\frac{\tilde{E}_{inc}(\omega)}{\sqrt{377\,\Omega}} \tag{B.4}$$

Let us now compare the above equation to the standard equation for reception. Thus, we convert (A.1) of this paper into the frequency domain, obtaining

$$\frac{\tilde{V}_{rec}(\omega)}{\sqrt{50\,\Omega}} \;=\; \tilde{h}_N(\omega)\frac{\tilde{E}_{inc}(\omega)}{\sqrt{377\,\Omega}} \tag{B.5}$$

where $h_N(\omega)$ is the normalized antenna impulse response expressed in the frequency domain. We combine the above two equations to obtain

$$G_{eff}(\omega) \;=\; \frac{4\,\pi}{\lambda^2}\,|\,\tilde{h}_N(\omega)\,|^2 \;=\; \frac{4\,\pi\, f^2}{c^2}\,|\,\tilde{h}_N(\omega)\,|^2 \tag{B.6}$$

This formula allows us to convert our time domain normalized impulse response to effective gain. Effective gain is simply absolute gain, as defined by IEEE Std. 145, multiplied by a transmission coefficient that accounts for mismatch between the antenna and feed line, or

$$G_{eff}(\omega) = G(\omega)\left[1 - |S_{11}|^2\right] \tag{B.7}$$

This is sometimes a more useful version of gain than simple antenna gain (or absolute gain) as defined by IEEE Std. 145

Antenna Factor

A quantity that is sometimes useful is the antenna factor, which is defined as

$$AF(\omega) = \left|\frac{\tilde{E}_{inc}(\omega)}{\tilde{V}_{rec}(\omega)}\right| \tag{B.8}$$

Note that this inversion assumes that the angle of incidence is known. In addition, it assumes that the antenna is symmetrical, so it has no cross-polarized response. If we convert the receive equation of (A.1) to the frequency domain, we have

$$\frac{\tilde{V}_{rec}(\omega)}{\sqrt{50\,\Omega}} = \tilde{h}_N(\omega)\,\frac{\tilde{E}_{inc}(\omega)}{\sqrt{377\,\Omega}} \tag{B.9}$$

Comparing the two above equations, we have

$$AF(\omega) = \sqrt{\frac{377\,\Omega}{50\,\Omega}}\,\frac{1}{\left|\tilde{h}_N(\omega)\right|}$$

$$AF(\omega) = \frac{2.75}{\left|\tilde{h}_N(\omega)\right|} \tag{B.10}$$

Combining the above with equation (B.6) gives an alternate expression as

$$AF(\omega) = \frac{9.73}{\lambda\,\sqrt{G_{eff}(\omega)}} \tag{B.11}$$

Appendix C: Return Loss (S_{11}) Calculation

In order to convert between effective gain and standard gain, we require the return loss, or S_{11} of the antenna, as shown in equation (A.10). We provide here the details of how to measure S_{11} in the time domain.

We obtain S_{11} from a pair of TDR measurements. From a TDR of the antenna, we obtain an observed reflection coefficient into the antenna, $\rho(t)$. From a TDR of the shorted feed cable we obtain a second reflection coefficient, $\rho_s(t)$, which provides the stimulus at the antenna input. The S_{11} parameter is the frequency domain transfer function:

$$S_{11}(\omega) = \frac{\text{FFT}\,[\rho(t)]}{\text{FFT}\,[\rho_s(t)]} \tag{C.1}$$

where FFT is the Fast Fourier Transform. We trim the leading edge of the time domain waveforms $\rho(t)$ and $\rho_s(t)$, so that each waveform begins at about the same point on the feed cable, where $\rho \approx \rho_s \approx 0$. At late time, neither ρ nor ρ_s return approximately to zero, as we require for application of the common FFT. If we used a cosine-squared-taper to force the late time to zero, we would introduce numerical artifacts.

We avoid the problem with the late-time behavior of the reflection coefficient by making use of the Fourier transform differentiation theorem:

$$\text{FFT}\left[\frac{d}{dt}\rho(t)\right] = j\omega\,\text{FFT}\left[\rho(t)\right] \tag{C.2}$$

With this relationship, we obtain

$$S_{11}(\omega) = \frac{\text{FFT}\left[\dfrac{d}{dt}\rho(t)\right]}{\text{FFT}\left[\dfrac{d}{dt}\rho_s(t)\right]} \tag{C.3}$$

The advantage of this formulation is that $d/dt\,[\rho(t)]$ is more likely to be close to zero at late times than is $\rho(t)$. This is certainly true in the case of the derivative of the reflection from the short, $d/dt\,[(\rho_s(t)]$. The end of the two derivative waveforms are smoothly tapered to zero using a cosine-squared taper before carrying out the frequency domain division. The frequency domain division is actually a deconvolution, which requires special care as described in Appendix D.

Appendix D: Numerical Details: Deconvolution and Complex Square Root

In Appendix A we implemented a number of divisions in the frequency domain, which are the equivalent of time domain deconvolutions. There is no pure closed-form deconvolution method that is widely accepted and numerically stable, so we provide here our method for implementing the deconvolution. In addition, one must use care when implementing the complex square root in Appendix A, and we describe here the details of how we have done so.

The first problem in deconvolution occurs when one attempts to divide by a complex number with a small magnitude. To solve this, we apply to the raw ratio, $H(f)$, an operation know as "limiting the ratio." In doing so, we limit $|H(f)|$ to be no smaller than H_{min}. Thus, we use the limited form of the raw ratio, $H_{lim}(f)$, calculated as

$$H_{\lim}(f) \ = \ \frac{H(f)}{|H(f)|}\sqrt{H_{\min}{}^2 + |H(f)|^2}$$

$$H_{\min}(f) \ = \ \text{Max}(|H(f)|) \times q \tag{D.1}$$

where q is the "limit ratio." The effect of this procedure is that the magnitude of the raw ratio is adjusted to be no smaller than q times the maximum of the raw ratio, while preserving the phase. Typically, the limit ratio, q, is set to 0.01. It was a bit surprising to us that a nonlinear operation such as this would consistently provide good results, but that has been our experience over several years of testing.

The next step in the deconvolution is to apply a low-pass filter to the limited ratio. The filter we normally use is a modified (simplified) Butterworth filter described by

$$G(f) \ = \ \frac{1}{1 + (f/f_o)^{2N}} \tag{D.2}$$

where f_o is the cutoff frequency of the filter, and N is the order of the filter. This filter is a bit simpler to calculate than a true Butterworth filter, but in our tests it seemed to work just as well. Note that unlike a true Butterworth filter, the above filter is non-causal, i.e., its inverse Fourier transform does not begin at time $= 0$. This had originally concerned us, but repeated numerical experiments demonstrated no practical advantage to the true Butterworth filter.

Finally, we note that some care must be exercised when implementing the complex square root function in equation (A.6). One loses phase information when the phase wraps, so phase wraps must be avoided. The simplest way to fix the problem is to unwrap the phase before taking the square root. In practice, this means that we implement an inverse Fourier transform on the frequency domain signal just before taking the square root. We then adjust the delay on the resulting time domain waveform so that the peak occurs at time $= 0$, which removes as many of the phase wraps as possible. We then Fourier transform the result and take the complex square root, making sure that the cutoff frequency of the low-pass filter is set low enough to exclude any remaining phase wraps. Finally, the time delay is restored from its earlier value.